BEHAVIOUR OF LARGE SCALE RIGID MODEL PILES UNDER INCLINED LOADS IN SAND

JAE SHIK JOO

BEHAVIOUR OF LARGE SCALE RIGID MODEL PILES

UNDER INCLINED LOADS IN SAND

BY

© JAE SHIK JOO, B.Eng.

A thesis submitted to the School of Graduate

Studies in partial fulfillment of the

requirements for the degree of

Master of Engineering

Faculty of Engineering & Applied Science
Memorial University of Newfoundland

April 1985

St. John's Newfoundland Canada

To my wife and mother

ABSTRACT

Attention has been directed towards the stability of offshore structures since the discovery of oil under the sea bed in the 1920's. Especially important in this field of engineering are the large lateral loads from wind, waves, and currents in conjunction with vertical loads. This combination of loads creates the need to analyze systems exposed to large inclined loads.

The scope of this research is to understand the behaviour of a vertical rigid short pile under inclined loads in dense sand. The pile behaviour under inclined loads has been examined in the laboratory using relatively large circular model piles of 75 mm, 90 mm, and 102 mm diameters and a square pile of 73 mm width. These model piles were instrumented with pressure transducers and load cells in order to measure soil pressures. The piles were tested with vertical, inclined, and horizontal loads using a computerized data acquisition system. For these model pile tests a suitable laboratory test frame and a circular steel soil container were designed and assembled.

As part of the comprehensive test program, the piles were first subjected to vertical loads. The bearing capacity factor N_q was found to be constant with depth and consistently smaller than that predicted by various existing theories. For a smooth circular pile the pull out resistance can be estimated as the sum of one half the downward skin friction plus the weight of the pile.

For computing the ultimate lateral load on circular piles, modification of existing theories is necessary to take into account the parabolic soil pressure

variation across the projected pile diameter, rather than the rectangular distribution which is conventionally assumed.

The ultimate load capacity under inclined loads does not decrease uniformly with load inclination. For angles up to about 35°, the ultimate load capacity is larger than the vertical load capacity.

ACKNOWLEDGEMENTS

This thesis was completed at the Faculty of Engineering and applied Science, Memorial University of Newfoundland. The project was partially funded by the Natural Sciences and Engineering Research Council of Canada. The author wishes to acknowledge the receipt of a Memorial University Fellowship and a graduate supplement during the period of this study.

The author appreciates very much the advice, guidance, and careful review of the manuscript by his supervisor Dr. T. R. Chari, Professor and Associate Dean of Engineering. Thanks are due to Dr. G. R. Peters, Dean of Engineering for facilities provided and to Dr. F. A. Aldrich, Dean of Graduate Studies for his help and encouragement.

The author expresses his special appreciation to Mr. C. Roy Dawe and Mr. K. S. R. Prasad for advice and encouragement and to Mr. M. Ruprai for his help in the experiments. Thanks are due to Mr. P. Robinson, Mr. J. Andrews and their colleagues at the University Technical Services for assembling the experimental facilities. The help of Mr. A. Bursey and Mr. C. Ward is much appreciated.

Table of Contents

List of Tables

List of Figures

LIST OF SYMBOLS

The symbols used in this thesis conform generally to the recommendation of the Canadian Geotechnical Society (Barsvary et al. 1980). They are also defined where they first appear in the text of the thesis.

A_p	Area of pile base (L^2)
A_s	Area of pile shaft embedded in the soil (L^2)
B	Diameter or width of pile (L)
C_U	Uniformity coefficient (dimensionless)
D	Depth of pile beneath ground (L)
D_n	n percent grain size (L)
D_R	Relative density (dimensionless)(formerly called specific gravity)
E	Modulus of linear deformation (FL^{-2})(modulus of elasticity)
e	eccentricity (L)
F	Factor of safety (dimensionless)
H	Lateral force applied to a pile (F)
I	Moment of inertia (L^4)
I_D	Density index (%)
K_a	Coefficient of active earth pressure (dimensionless)
K_o	Coefficient of earth pressure at rest (dimensionless)
K_p	Coefficient of passive earth pressure (dimensionless)
$\left.\begin{matrix}K_q\\K_c\end{matrix}\right\}$	Coefficients of lateral earth pressure at arbitrary depth (dimensionless)
K_s	Average coefficient of earth pressure on the

	pile shaft (dimensionless)
L	Length of pile (L)
N	S. P. T. blow count (Blows/0.3 m)
N_c, N_q, N_r	Bearing capacity factors (dimensionless)
n_h	Horizontal coefficient of subgrade reaction (FL^{-3})
Q	Applied axial load (F)
Q_a	Ultimate axial load (F)
Q_n	Ultimate lateral load (F)
Q_u	Ultimate inclined load (F)
Q_p	Point resistance force (F)
Q_s	Total shaft resistance (F)
Q_s'	Total pull out resistance (F)
q_c	Static cone point resistance (FL^{-2})
q_p	point resistance pressure (FL^{-2})
q_{pn}	Net point resistance pressure (FL^{-2})
q_s	Unit shaft resistance (FL^{-2})
T	stiffness factor (L)
w	Water content (%)
α	Inclination of load (^{o}(deg))
γ	Unit weight (FL^{-3})
γ_d	Dry unit weight (FL^{-3})

δ	Angle of wall friction (^{o}(deg))
ρ	Density (ML^{-3})
$\rho_{d(max)}$	Maximum dry density (ML^{-3})
$\rho_{d(min)}$	Minimum dry density (ML^{-3})
σ	Total normal stress (FL^{-2})
σ'	Effective normal stress (FL^{-2})
τ	Shear strength (FL^{-2})
ϕ	Apparent angle of internal friction (^{o}(deg))

Chapter 1
INTRODUCTION

1.1. General

Piles have been commonly used to transfer structural loads through weak soil strata to a more suitable soil stratum at greater depths. The loads on structures could be vertical, lateral or a combination of these. Generally for most buildings, the vertical load is predominant. However, lateral load is an important factor in the design of tall structures, piers, bridge abutments, poles with large sign boards, retaining walls on land and for deep water ports, light stations, offshore structures, nuclear power plants, and harbour facilities. Lateral forces may be caused by the wind, waves, currents, ice movement, berthing ships, earthquake loading, etc.

Depending on the inclination of the pile axis to the plumb line, piles can be classified as vertical or batter piles. Often, vertical piles are used to resist vertical loads, and batter piles are separately designed for the lateral loads. However, with the advent of offshore structures subjected to large lateral loads there is an increased need for the design of vertical piles subjected to inclined loads.

One of the early field tests of vertical piles subjected to inclined loads was conducted by Evans (1953). The piles were subjected to a constant vertical load with increasing horizontal loads at the site of Sepulveda dam, California. Since then, investigation of piles subjected to inclined loads has been mostly laboratory research in which small diameter model piles have been examined (Awad and Petrasovits 1968, Meyerhof and Ranjan 1972, Meyerhof et al. 1981, 1983). Meyerhof et al. (1981) have proposed an interaction equation for estimating the ultimate load under inclined loads based on test results of a 12.5 mm diameter model pile. This equation was verified subsequently using a 75 mm diameter instrumented pile (Chari and Meyerhof 1983).

1.2. Scope of the investigation

This investigation is a continuation of the earlier efforts to understand the behaviour of short piles subjected to inclined loads, using model piles of larger diameter.

The laboratory facilities were designed and assembled for conducting the model pile tests. A galvanized corrugated steel tank 1.8 m diameter and 2 m high was suitably modified to enable the preparation of samples of sand with different densities. Instrumented model piles of 73 mm, 90 mm, 102 mm diameters, and 73 mm square were used and the piles were loaded to the ultimate bearing capacity of the soil with vertical, inclined, and horizontal loads. The inclinations of loads were at 30, 45, and 60 degrees.

The objectives of this investigation are:

(1) to compare the predicted ultimate bearing capacity of piles with the measured value,

(2) to study the variation of the ultimate bearing capacity of piles with the inclination of loads, and

(3) to analyze the results in the light of available theoretical and empirical methods of prediction.

A brief review of literature is presented in Chapter 2. The details of the experimental set up and test procedures are given in chapter 3. Chapter 4 deals with experimental results and discussion. Chapter 5 gives the summary, conclusions, and recommendations for further research relevant to this study.

Chapter 2
REVIEW OF LITERATURE

2.1. General

Piles are classified in a number of ways depending on their function, composition, and method of installation. A definition diagram showing the commonly used nomenclature for pile foundations is given in Figure 1.

A vertical pile has its axis coinciding with the plumb line while a batter pile has its axis inclined to the plumb line. Vertical piles are usually used to resist dead and live loads, uplift due to swelling and frost expansion of soil, and forces due to hydrostatic pressure beneath the base of a structure. Batter piles are commonly used to resist inclined or large lateral loads.

A short pile is relatively rigid and rotates as one unit under lateral loads while a long pile is relatively flexible and acts like a beam under lateral loads. The criteria for the classification of short and long piles is given in Figure 1. The design length of a pile mainly depends on the profile of the subsoil and the type and magnitude of loading.

There is an extensive amount of available literature on axially and laterally loaded piles. Generally, the vertical capacity of a pile is dictated by the ultimate

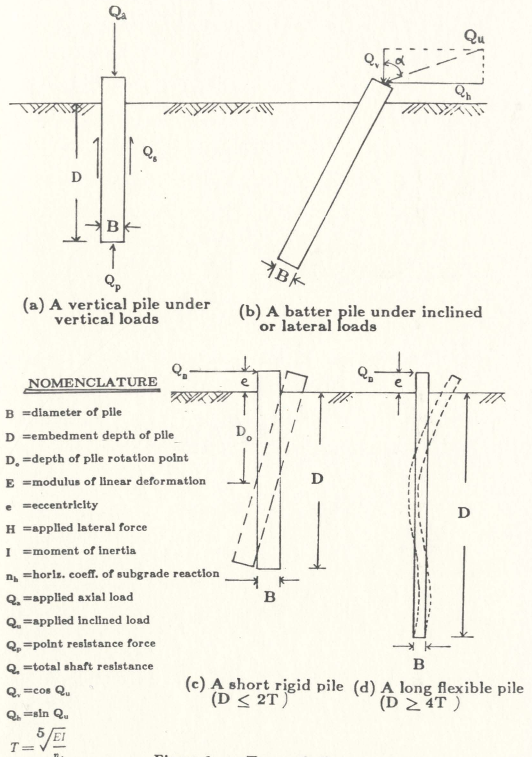

Figure 1: Types of piles

bearing capacity of the soil. The ultimate bearing capacity in turn may be defined as the maximum load which the pile can support without undergoing significant settlements. The ultimate bearing capacity of vertical piles under axial loads in sands is generally evaluated using soil properties such as its density and the angle of shear resistance (Terzaghi 1943, Meyerhof 1951, Vesic 1963). The ultimate lateral load of vertical short rigid piles is generally computed based on lateral earth pressure theories (Brinch Hansen 1961, Broms 1964, Petrasovits et al. 1972, Meyerhof et al. 1981), and the ultimate lateral load of a long flexible pile can be evaluated using the theory of elasticity (Rowe 1955, Matlock and Reese 1962, Broms 1964, Poulos 1971).

Literature on the ultimate capacity of vertical rigid piles subjected to inclined loads is somewhat limited. One of the present methods to compute the ultimate capacity under inclined loads is to use an interaction equation (Meyerhof 1981). A brief review of the existing theories of vertical and lateral ultimate capacity of short rigid piles is presented here.

2.2. Vertical piles under axial loads

The ultimate bearing capacity Q, of a vertical pile under an axial load (Figure 1a) is generally expressed as the sum of point resistance force Q_p, and total shaft resistance Q_s, as follows:

$$Q = Q_p + Q_s$$

$$= q_p A_p + q_s A_s \qquad (1)$$

where q_p is the point resistance pressure,

q_s denotes the average unit shaft resistance,

A_p is the area of pile base, and

A_s is the area of embedded pile shaft.

The point resistance pressure q_p, and the average unit shaft resistance q_s, are functions of several parameters but mainly depend on the type of soil, the density of soil, the angle of friction, and the physical properties of the pile. For practical purposes, Equation 1 is formulated on the premise that the two components q_q and q_s are independent of each other. In fact, for piles driven into cohesionless soils there is some interdependence between the two components (Kezdi 1957), but this small influence is generally neglected (Broms 1966). The magnitudes of the two components Q_p and Q_s in cohesionless soil may be intuitively expected to be proportional to the embedded depth, but according to laboratory and field test results, the proportionality cannot be satisfied beyond the critical depth below which the ultimate load remains relatively constant (Kerisel 1964, Vesic 1963, Vesic 1964, Tavenas 1970). The relative magnitudes of Q_p and Q_s depend on the type of soil and the method of installation of the pile.

Based on the method of placement, vertical piles may be classified into two broad categories. A pile driven into the soil is classified as a displacement pile. A pile which is placed by removing an equal volume of the soil is generally called non-displacement pile (sands) or a bored pile (clays). The capacity of the pile is predominantly the end bearing resistance for a non-displacement (bored) pile, while it is the sum of the end bearing and side frictional resistance for a displacement (driven) pile.

The ultimate bearing capacity of a pile Q, can be estimated by several methods and the most commonly used are:

(1) based upon bearing capacity theories,

(2) from the results of in-situ tests, and

(3) prototype pile load tests.

The first two methods which are relevant to this thesis will be reviewed in the following sections.

2.2.1. Estimation of Q based on bearing capacity theories

Point resistance force, Q_p

Most of the present solutions for the point resistance force of pile foundations are derived using Prandtl's (1920) and Reissner's (1924) general bearing capacity theories based on the assumption of weightless material, and Ohde's (1938) theory considering the weight of the material. The resulting point resistance pressure is expressed by the following general equation.

$$q_p = (cN_c + \gamma D N_q + \frac{B}{2} \gamma N_\gamma) \qquad (2)$$

where q_p is the point resistance pressure of the cross-section area of pile,

N_c, N_q, N_γ are the bearing capacity factors,

B is the diameter of pile,

γ is the effective unit weight of soil at the level of pile tip,

c is the cohesive strength of soil, and

D is the vertical distance between the ground surface and the level of pile tip.

For deep foundations in cohesionless soils, the first term will be zero and the third term is negligibly small in comparison to the second term. Hence, Equation 2 can be simplified as:

$$q_p = \gamma DN_q \tag{3}$$

When it is necessary to consider the weight of the pile, the net point resistance pressure q_{pn}, of a pile can be determined based on the assumption that the unit weight of pile material is equal to that of soil.

$$q_{pn} = \gamma D(N_q - 1) \tag{4}$$

Equations 3 and 4 indicate that the bearing capacity of a pile varies with the bearing capacity factor N_q, which depends on the deformation characteristics of the soil. Vesic (1967, 1977) has summarized the various theoretical approaches to simulate the failure mechanism of soil as shown in Figure 2. The corresponding N_q values in sand as suggested by various investigators are reproduced in Figure 3 and Table 1.

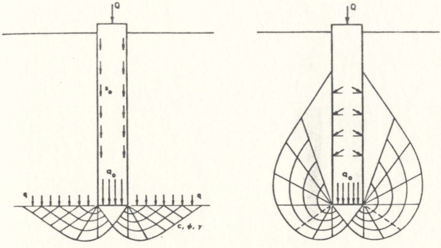

Prandtl (1921)
Reissner(1924)
Caquot (1934)
Buisman (1935)
Terzaghi(1943)

DeBeer (1945)
Jaky (1948)
Meyerhof(1951)

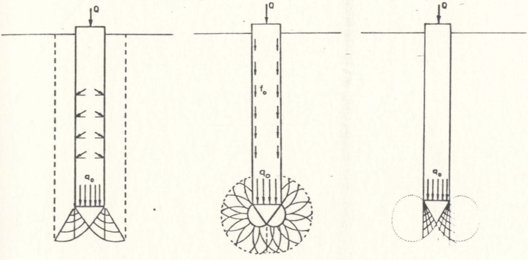

Berezantsev and
Yaroshenko (1962)
Vesic (1963)

Bishop, Hill & Mott (1945)
Skemton, Yassin &
Gibson(1953)

Vesic (1977)

Figure 2: Assumed failure patterns of soil

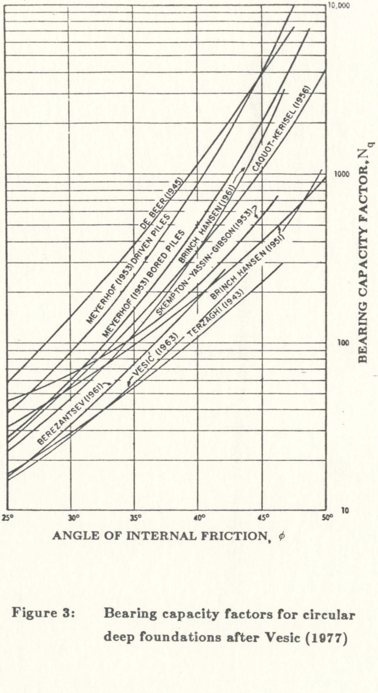

Figure 3: **Bearing capacity factors for circular deep foundations after Vesic (1977)**

TABLE 1

Experimental values N_q in sand

SAND COMPACTNESS	DENSITY INDEX (%)	N_q	
		DRIVEN PILES	BORED PILES
Very dense	>80	60-200	40-80
Dense	60-80	40-80	20-40
Medium	40-60	25-60	10-30
Loose	<40	20-30	5-15

After Vesic(1977), higher values apply to shorter piles.

It is reported (Norlund 1963, Broms 1966, Vesic 1964, 1967) that in practice, the N_q values of Berezantzev are found to correlate well with the measured values. However, Coyle and Castello (1979) suggested that Terzaghi's N_q values for general shear failure were found to fit their experimental results.

The point resistance pressure q_p, has been normally found to increase up to a certain depth beyond which any increase in D does not result in significant increase of q_p. This depth has been normally designated as the critical depth. Kerisel (1964), and Meyerhof (1976) reported that the value of N_q in sand increases with depth and reaches its maximum value at less than half of the critical depth. While Berzantsev et al. (1961), and Drugunoglu & Mitchell (1973) found that N_q decreases with increasing D/B ratio, Vesic (1977) concluded that N_q is a constant, independent of the depth.

In addition to the depth, N_q depends on many factors such as density of the soil, overburden pressure, shape of the pile and method of installation. For driven piles the change of density of soil due to driving a pile has to be taken into account to evaluate the ultimate load capacity of the pile. However, as mentioned earlier, the available theories are based on the assumption that the soil density during pile driving is not changed. In fact, the density index increases for driven piles in sand except in very dense sand, and therefore the angle of internal friction ϕ_2, after driving the piles is larger than the initial internal angle of friction ϕ_1. The relationship between ϕ_1 and ϕ_2 in sand has been suggested as follows (Kishida and Meyerhof 1965):

$$\phi_2 = \frac{(\phi_1 + 40)}{2} \tag{5}$$

Equation 5 implies that there is no change in density index for soils with an internal friction angle of 40°.

Based on the failure mechanism shown in Figure 2e, Vesic (1977) has given the following equation for q_p:

$$\begin{aligned} q_p &= \sigma_o N_\sigma \\ &= \frac{(1 + 2K_o)\gamma D}{3} N_\sigma \end{aligned} \tag{6}$$

where K_o is the coefficient of lateral earth pressure at rest.

σ_o is the mean normal stress at pile tip,

γ is the unit weight of soil,

D is the embedded pile length, and

N_σ is the bearing capacity factor for mean normal stress term and is a function of compressibility as well as internal friction angle of soil.

The point resistance force Q_p can thus be computed as the product of q_p and the area of the pile base A_p.

Total shaft resistance, Q_s

For deep foundations the total shaft resistance Q_s, can be defined as the resistance to the sliding of a rigid body relative to the surrounding soil and is generally expressed by two components: (1) adhesion, and (2) friction, dependent on normal stresses.

The unit shaft resistance of driven piles q_s, at any depth Z below the ground surface can be calculated from Mohr-Coulomb's theory of rupture as follows:

$$q_s = c_a + K_s \sigma' \tan \delta \qquad (7)$$

where c_a is the undrained pile-soil cohesion,

K_s denotes the coefficient of earth pressure on the pile shaft,

δ is the angle of shaft friction between soil and pile material,

σ' is the average effective overburden pressure at any point and defined as the product of γ' and Z,

γ' is the effective unit weight of soil,

For piles in cohesionless soils the value of c_a is zero. Equation 7 can be rewritten integrating along the embedded pile length for the total shaft resistance Q_s, as follows (Dorr 1922, Meyerhof 1951, Norlund 1963).

$$Q_s = \frac{1}{2} K_s \gamma' D \tan \delta A_s \qquad (8)$$

where A_s is the total area of embedded pile shaft,

D is the embedded depth of pile, and

K_s is the average coefficient of earth pressure on the pile shaft.

The magnitude of coefficient K_s in Equation 8 depends mainly on the initial relative density, the displacement volume of the pile, the shape of pile, and the method of pile installation. However, for practical purposes the averaged values of K_s can be taken for piles driven into cohesionless soil. The coefficient K_s for driven steel piles has been suggested as 1.0 for dense sand and 0.5 for loose sand regardless of pile type and roughness of the pile surface (Meyerhof 1951, Broms 1966, Coyle and Castello 1979).

The angle of friction δ, between the soil and the shaft has been suggested based on experimental data as 0.54 ϕ for smooth steel piles and 0.76 ϕ for rusted steel piles where ϕ represents the angle of internal friction for the soil (Pontyondy, 1961). Other researchers have given the skin friction angle δ as 20° for steel piles assuming that the value of δ is independent of the density index of the soil surrounding the pile (Broms 1966, Craig 1978, Tomlinson 1981).

2.2.2. Estimation of Q based on in-situ tests

The vertical capacity of piles can be also estimated based on in-situ tests such as the standard penetration test (SPT) and the cone penetrometer test (CPT). Both types of tests are routinely done as part of site investigations.

The standard penetration test can be used to determine the ultimate bearing capacity of piles in cohesionless soils. This ultimate bearing capacity Q, in sands has been expressed as (Meyerhof 1956, 1976):

$$Q = \{ 4\,N A_p + \frac{N A_s}{50} \} \; (100\ kN/m^2) \tag{9}$$

where N denotes the average penetration resistance near the pile tip (blows/0.3 m),

A_p represents the area of the pile base, and

A_s denotes the area of embedded pile shaft.

It should be noted that the accuracy of the above estimate depends on the reliability of the blow count N. As is common knowledge, the standard penetration test is not generally used for cohesive soils and Equation 9 is valid only for cohesionless materials.

If the ratio of depth to diameter of the pile is less than 10, the point resistance pressure q_p, can be expressed as (Meyerhof 1956):

$$q_p = \frac{4ND}{10B} \quad (100\ kN/m^2) \tag{10}$$

The cone penetrometer test in cohesive and cohesionless soils has been correlated with the ultimate bearing capacity of piles. The ultimate bearing capacity Q, of piles in cohesionless soil has been given as (Meyerhof 1956):

$$Q = q_c A_p + 0.005\, q_c A_s \tag{11}$$

where q_c denotes the average static cone point resistance, and

A_p is the area of pile, and

A_s is the area of embedded pile shaft.

Equation 11 has been derived on the assumption that the point resistance pressure of the pile is equal to the average static cone point resistance q_c, over a depth of 4 pile diameters above and one pile diameter below the anticipated depth of the pile tip (Meyerhof 1956, Menzenbach 1961). It is also assumed that the unit shaft resistance is equal to 0.5 % of the average static cone point resistance (Meyerhof 1956, 1976).

If the depth of foundation is less than 10 times the pile diameter, the point resistance pressure q_p, can be expressed as:

$$q_p = q_c \, D \, / \, 10B \tag{12}$$

where D is the embedded pile length, and

B represents the width or diameter of the pile.

Subsequent work shows good correlations for pile diameters less than 50 cm (Kerisel 1961). However, the total shaft resistance on concrete piles was found to be greater than that given by Equation 13 (Mohan et al. 1963). Tomlinson (1977) has given a slightly different approach in which the values of K_s and ϕ can be estimated from cone penetrometer tests. The suggested values are given in Table 2, and from these, the ultimate bearing capacity Q, can be estimated as:

$$Q = q_c \, A_p + 0.5 \, K_s \, \gamma D \tan \delta \, A_s \tag{13}$$

TABLE 2

ϕ and K_s corresponding to the various values, q_c

q_c (g/cm^2)	ϕ (deg.)	K_s
0-50	28-30	Low relative density
50-100	30-36	Medium relative density
> 100	>36	High relative density

After Tomlinson (1977)

2.3. Vertical Rigid Piles under Lateral Loads

Piles are generally classified as short and long based on two criteria. A short free-headed pile having a depth/diameter (D/B) ratio of 10-12 will fail by rotation developing passive resistance on opposite faces above and below the point of rotation. The pile rigidity is also related to a stiffness factor T which is expressed as (Davison and Prakash 1963, Broms 1964, Tomlinson 1977):

$$T = \left(\frac{EI}{n_h} \right)^{1/5} \tag{14}$$

where EI is the stiffness of the pile, and

n_h is the coefficient of horizontal subgrade reaction.

The length of the pile is to be less than about 2T for behaviour as a short rigid pile and greater than 4T for behaviour as a long elastic pile. Theoretical analyses of the behaviour of short rigid piles have been presented in published literature (Brinch Hansen 1961, Christensen 1961, Broms 1964, Petrasovits and Awad 1972, Adams and Radhakrishna 1973, Meyerhof et al. 1976, 1981). At failure, it is assumed that a short rigid pile rotates as a unit body, and that the ultimate lateral resistance of the soil will be reached before a structural failure of the pile.

The exact pressure distribution on a rigid pile subjected to lateral loads is nonlinear. However, presently available analytical methods are based on a simplified assumption of the true pressure distribution as shown in Figure 4.

Brinch Hansen (1961) has suggested an equation for the lateral earth

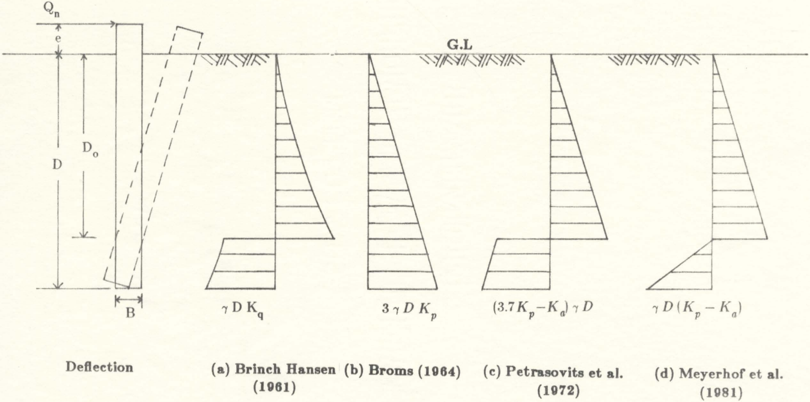

Figure 4. Assumed soil pressure distribution under lateral loads

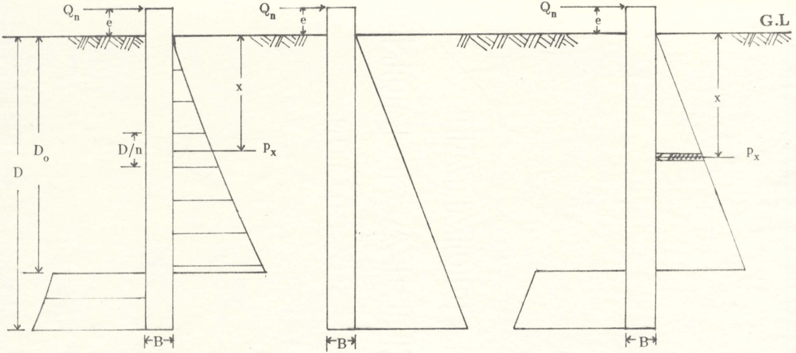

(a) Brinch Hansen (1961) (b) Broms (1964) (c) Petrasovits et al. (1972)

Figure 5. Calculation of Q_n

pressure p_x, at depth x based on the assumption of nonlinear soil pressure distribution as shown in Figure 4a. The lateral earth pressure p_x, at depth x is expressed as:

$$p_x = c\,K_c + \gamma\, x\, K_q \qquad (15)$$

where c is the cohesive strength of soil,

γ is the unit weight of soil,

x is the arbitrary depth below the soil surface, and

K_c, K_q are the earth pressure coefficients dependent on ϕ and the ratio of embedded pile depth to pile diameter (D/B).

For driven piles in cohesionless soil, Equation 15 can be simplified by taking the value of c as zero:

$$p_x = \gamma\, x\, K_q \qquad (16)$$

Assuming the earth pressure distribution as shown in Figure 5a, the depth of rotation point D_o, can be found by trial and error by taking moments about the line of application of the load as follows:

$$\Sigma M(=0) = \sum_{x=0}^{D_o} P_x \frac{D}{n}(e+x)B - \sum_{x=D_o}^{D} P_x \frac{D}{n}(e+x)B \qquad (17)$$

Knowing D_o, the ultimate lateral load Q_n, can be calculated taking moments about D_o:

$$Q_n (e + D_o) = \sum_{x=0}^{D_o} P_x \frac{D}{n} B(Do-x) + \sum_{x=D_o}^{D} P_o \frac{D}{n} B(x - D_o) \qquad (18)$$

where n is the convenient number of horizontal elements of embedded pile length,

e is the eccentricity of the applied load above the soil surface, and

B is the diameter or width of pile.

Another approach has been given by Broms (1964) who suggested a simple equation based on the following assumptions for calculation of ultimate lateral resistance of rigid vertical free headed piles in cohesionless soil:

(1) Maximum lateral earth pressure is equal to three times the Rankine passive earth pressure at failure assuming that the pile surface is frictionless.

(2) The active pressure along the pile is negligible.

(3) The shape of the pile cross-section has little effect on the earth pressure distribution.

(4) A large lateral reaction develops at the pile tip in the same direction as the applied load.

Assuming a lateral earth pressure distribution as shown in Figure 5b, the ultimate lateral resistance Q_n, can be expressed by employing equilibrium conditions.

By taking moments about the tip of pile,

$$Q_n = \frac{(0.5\,\gamma\,D^3\,K_p\,B)}{(e+D)} \tag{19}$$

where e is the eccentricity of the applied load above the soil surface,

D is the embedded pile length,

γ is the unit weight of soil,

K_p is the coefficient of the Rankine passive earth pressure

defined as $K_p = (1+sin(\phi))/(1-sin(\phi))$

ϕ is the internal friction angle of soil, and

B is the diameter or width of pile.

In the above theory, the assumed triangular earth pressure distribution is quite different from the actual pressure distribution and gives relatively higher values than published experimental results (Poulos 1978).

Petrasovits and Awad (1972) extended Broms' method for rigid piles in cohesionless soil by assuming that the rotation point occurs along the pile rather than at the pile tip. They assumed that at the back side of the pile the earth pressure is equal to the Rankine active earth pressure (Rowe 1956) and the full passive earth pressure is equal to 3.7 times the Rankine passive earth pressure. Based on the assumed earth pressure distribution as shown in Figure 5c, the ultimate lateral resistance Q_n, can be calculated using the horizontal force equilibrium, and moment equilibrium:

$$Q_n = \frac{1}{2}\,(3.7\,K_p - K_a)\,\gamma\,B\,D^2\,(2\,R^2 - 1) \tag{20}$$

$$Q_n = \frac{1}{3}\,(3.7\,K_p - K_a)\,\gamma\,B\,D^3\,(1 - 2\,R^3)/\,e \qquad (21)$$

The following equation can be derived from Equations (20) and (21):

$$\frac{(2\,R^2 - 1)}{(1 - 2\,R^3)} = \frac{2}{3}\,\frac{D}{e} \qquad (22)$$

where $R = \frac{D_o}{D}$

K_p is the coefficient of Rankine passive earth pressure,

K_a is the coefficient of Rankine active earth pressure,

γ is the unit weight of soil,

B is the diameter or width of pile ,

D is the embedded pile length, and

e is the eccentricity of the applied load above the soil surface.

The depth of rotation point D_o, is obtained by trial and error. When D_o is found, Q_n can be calculated by Equations 20 and 21. Petrasovits and Awads (1972) indicate that the ratio D/e has little influence on the depth of the point of rotation. Results by the same authors show that this method is more suitable for short rigid piles rather than for long piles.

Meyerhof et al. (1981) have extended the theory of the ultimate lateral resistance of rigid vertical walls in layered soil to rigid vertical piles considering a shape factor for laterally loaded vertical piles. They suggest an equation for calculation of ultimate lateral resistance Q_n, based on the assumed earth pressure distribution as observed on rigid vertical walls as shown in Figure 4d.

From the equilibrium equation of moment about the point at ground surface and the equilibrium equation of lateral forces, the ultimate lateral resistance Q_n, is approximated by Meyerhof et al. (1981) as follows:

$$Q_n = B \gamma D^2 F_b K_b r_b S_{bu} \tag{23}$$

where γ is the unit weight of soil,

D is the embedded pile length,

K_b is the coefficient of earth pressure defined as:

$\tan^2(45 + \phi/2) - \tan^2(45 - \phi/2)$,

ϕ is the internal friction angle of soil,

F_b is the lateral resistance factor given by Meyerhof et al. (1981),

r_b is the reduction factor due to the moment Q_n e which is

defined as $r_b = 1/(1 + 1.4\frac{e}{D})$,

B is the diameter or width of pile, and

S_{bu} is the shape factor given by Meyerhof et al. (1981).

It may thus be observed that there are a number of theories for the prediction of lateral resistance of rigid piles and one would expect a variation in the results of these theoretical computations. Four of the available theories are used for the prediction purpose. In this thesis, a relative comparison will be made with actual measurements.

2.4. Inclined loads on piles

Two types of inclined loads on piles are discussed in the literature,

(1) piles subjected to pull out tests (Yoshimi 1965, Broms 1965, Awad and Petrasovits 1968, Meyerhof 1972), and

(2) piles subjected to push down tests (Evans 1953, Awad and Petrasovits 1968, Meyerhof and Ranjan 1972, Meyerhof et al. 1981,1983, Chari and Meyerhof 1983).

The latter types of test which are relevant to this thesis are discussed below.

One of the early contributions to research on piles subjected to inclined loads is the work of Evans (1953) in which field tests were done under constant vertical load and increasing horizontal loads for vertical and batter piles. However, published data were not enough to study the behaviour of a pile under inclined loads in terms of the ultimate bearing capacity of a pile.

For the behaviour of vertical rigid piles under inclined loads some tests were performed taking into account vertical eccentricity on three piles of different diameters ranging from 13mm to 35mm (Awad and Ptrasovits 1968). According to the experimental results, for a load inclination of 22.5^{o} the ultimate bearing capacity of three piles driven in uniform sand was a maximum and 16 to 35 % higher than the ultimate vertical bearing capacity. In these tests the ratio of vertical eccentricity to embedded pile length was 0.3, the density index I_D of the soil was 80%.

Meyerhof and Ranjan (1972) studied the behaviour of piles under inclined loads both theoretically and experimentally in uniform sand. Their investigation showed that the pile rotates only when the inclination of the load is more than 45^{o}. It has been reported that the ultimate bearing capacity of vertical rigid piles under inclined loads decreased with the inclination of loads. The results are based on the experiments with a 12.7 mm diameter pile pushed into uniform dense sand. Meyerhof and Ranjan (1972) have reported an equation for the estimation of the point resistance force Q_{pv}, under inclined loads as follows:

$$Q_{pv} = \gamma D N_q' A_b \tag{24}$$

where γ is the unit weight of the soil,

D is the embedded pile length,

N_q' is the bearing capacity factor relevant to load inclination given by Meyerhof et al. (1972), and

A_b is the area of the pile base.

Equation 24 implies that the point resistance force decreases with the load inclination. Meyerhof et al. (1981) have reported that the ultimate bearing capacity under inclined loads decreases with increasing inclination of loads to the vertical and have proposed an interaction equation for the determination of ultimate bearing capacity as follows:

$$\left(\frac{Q_u cos(\alpha)}{Q_a}\right)^2 + \left(\frac{Q_u sin(\alpha)}{Q_n}\right)^2 = 1 \tag{25}$$

where Q_u represents the ultimate bearing capacity of the pile under inclined loads,

Q_a denotes the ultimate axial load of the pile,

Q_n is the ultimate lateral load of the pile, and

α is the inclination of applied loads to vertical in degrees.

The experimental results with a 12.7mm diameter pile in layered uniform sand confirmed that the ultimate bearing capacity under inclined loads decreases with load inclination (Meyerhof et al. 1981). Earlier research showed that the ultimate capacity of a pile under inclined loads with a buried pile in compact sand did not decrease continuously with increasing load inclination (Meyerhof and Ranjan, 1973).

Chari and Meyerhof (1983) conducted laboratory tests with a relatively larger pile of 75mm diameter, and considered the depth of the point of rotation and the lateral earth pressure distribution under inclined loads in uniform dense sand: They compared the experimental results with the predicted values by the empirical interaction equation using Broms' theory for calculation of ultimate lateral resistance. The results indicated that there was good agreement between predicted and experimental results, and that the ultimate bearing capacity of the pile under inclined loads decreased continuously with increasing inclination of load.

A review of literature shows that there is a divergence of results in the literature. No agreement exists on the variation of ultimate capacity with inclination of load among researchers. This aspect is examined in some detail in this work and the results thereof presented in Chapter 4.

Chapter 3

EXPERIMENTAL FACILITIES and PROCEDURES

3.1. General

Most of the model tests reported in the literature have been conducted with piles of 12.5 to 35 mm in diameters. Test results with large diameter piles are sparse. Similarly there is not much data on test piles instrumented with pressure and load cells. In this study, circular piles of 73 mm, 90 mm, and 102 mm and a square pile of 73 mm were tested under vertical and inclined loads in sand. These piles were instrumented with pressure transducers and load cells.

The objectives of this experimental research are:

(1) study the variation of bearing capacity factor N_q, with relative depths,

(2) evaluate the pull out resistance of a vertical pile,

(3) study the variation of lateral earth pressure along the pile in order to evaluate the ultimate lateral load, and

(4) study the variation of the ultimate bearing capacity of a pile under vertical, inclined, and lateral loads and compare with theoretical computations.

To accommodate the physical size of the piles and the associated large forces, the soil container and the loading frame as shown in Figure 6 had to be suitably designed. Two screw jacks, one with a capacity of 178 kN and the other with 44.5 kN, were used in this study. The initial placement of the pile in the sand was done by pushing the pile vertically down using the jack of higher capacity. After pushing to the required depth, testing of the piles was done using the smaller jack with a swivel joint as shown in Figure 7. For all the different pile sizes, their corresponding lengths of embedment were chosen to ensure that the piles behaved as rigid piles.

A sketch of the different types of test piles is given in Figure 8. While only one length of embedment was used for the 73 mm and 90 mm diameter circular piles and the square pile, the 102 mm diameter pile was tested with three different lengths of embedment.

A total of 25 different types of tests were conducted using these piles as shown in Figure 8. A description of the test facilities and the experimental procedures is given below.

3.2. Experimental facilities

3.2.1. Soil container

The soil container is made out of a galvanized corrugated steel pipe (1.83 m dia. x 2.8 mm thick x 2 m high) as shown in Figure 6. The length and diameter of the container are governed by the anticipated zone of influence of a pile pushed into soil. This diameter should be large enough to avoid end effects of the container with a reasonable clearance. Figure 9 shows a typical pile pushed into sand and the type of densification that normally occurs around it. Table 3 is a summary of the published data on this phenomenon. The magnitude of dimensions a and b is dependent on the diameter of pile and the density of the sand.

In designing the size of the container, consideration was given to provide an adequate clearance between the walls of the container and the zone of soil densification. This extra clearance prevents confining effects of the walls on the test results and allows cone penetrometer testing of the relatively undisturbed soil after the pile is tested. The soil container used is large enough to test piles of up to 120 mm diameter with a 1400 mm embedded length. The structural strength of the container was also checked to verify the hoop tension due to the soil pressure inside. The soil container has two side openings with a chute and metal sliding doors, one near the bottom and the other 1 m above the base.

These openings facilitate easy removal of the soil after testing. A 2 mm thick steel plate is welded to the bottom of the container and the container rests

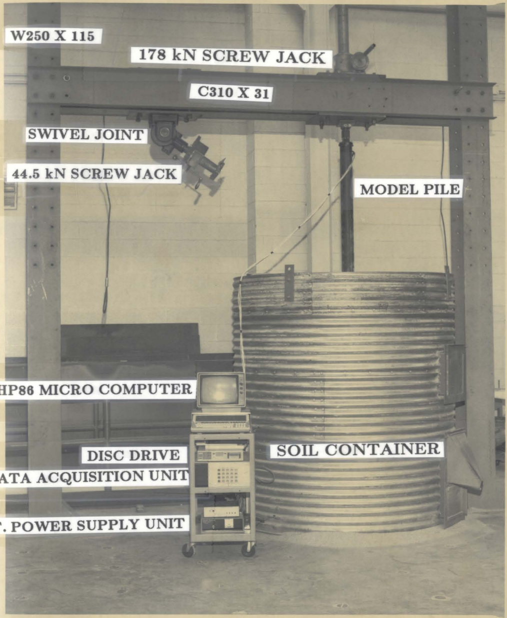

Figure 6: General experimental set up

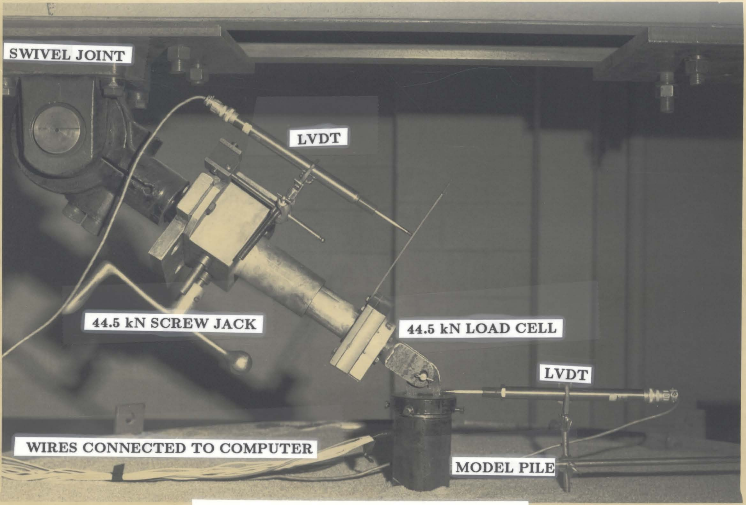

Figure 7: Configuration of loading system

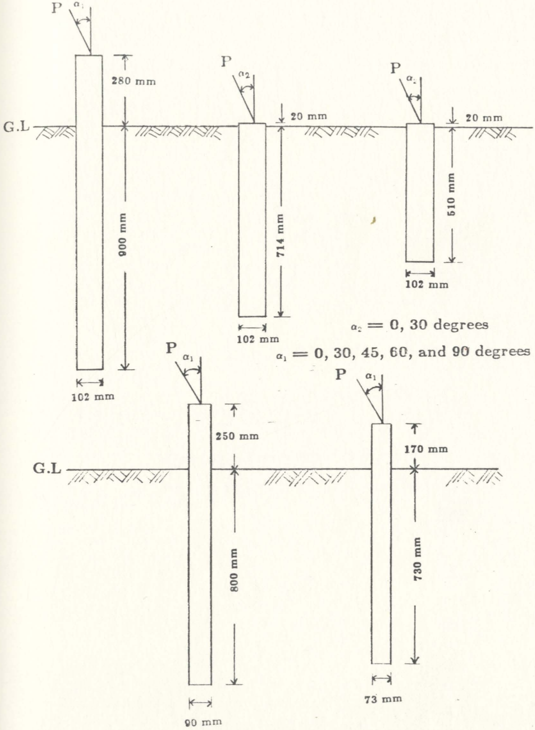

Figure 8: **Types of tests**

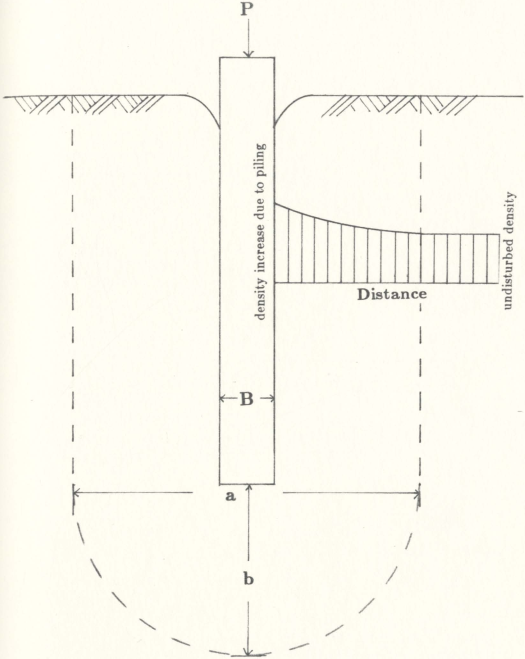

Figure 9: Influence zone of densification during placement of a pile

TABLE 3

Densification influence zone for driven pile in sand

INVESTIGATOR	DENSITY	INFLUENCE ZONE	
		a*	b*
Meyerhof(1959)	loose	6B* -8B	5B
Kerisel (1961)	dense	5B	
	General		3B
Robinsky & Morrison (1963)	loose	7B-9B	2.5B-3.5B
	medium	10B-12B	3B-4.5B
Kishida (1963, 1967)	loose	6B-8B	
	General		5B
Broms(1966)	General	7B-12B	3B-5B
Lamb & Whitman (1969)	General	16B	

a represents the width of densification zone.
b denotes the depth of densification zone below the tip.
B is the diameter of pile.

on a reinforced concrete floor. Adequate facilities are made so that the container can be lifted using an overhead crane and properly positioned relative to the loading frame.

A loading frame was designed and fabricated using two W 250 x 115 H sections for columns and a horizontal member made out of two C 310 x 31 channel sections as shown in Figure 6. The overall size of loading frame is 5.48 m high x 3.95 m wide. This frame is capable of withstanding vertical loads of 653 kN with a safety factor of 2 and horizontal loads of 16 kN applied at 2.1 m from the base of the frame.

3.2.2. Model piles

All the model piles are fabricated from standard, extra heavy black steel pipes. The pipes were split longitudinally and reassembled using suitably designed internal connecting rings to fasten the two halves. Pressure transducers were fitted in drilled holes and connected to electrical cables going through the center of the pile and finally coming out from the side at the top of the pile. The piles are pushed into sand manually using the jack of higher capacity which has a stroke of 1500 mm. Figures 10 and 11 show the model piles and some of the details of their dimensions. The physical properties of the piles are listed in Table 4.

3.2.3. Instrumentation and recording system

Lateral soil pressures on the piles were measured by two rows of diaphragm pressure transducers which were mounted flush with the pile wall. A detailed specification of the pressure transducers is given in Table 5. The total applied load was measured using a commercially available load cell located at the pile top. The point resistance force of each pile was measured using a full bridge strain gauge type load cell fabricated in-house. Figure 12 and 13 give the details of these load cells. Displacements were measured using dial gauges and linear variable differential transformers (LVDT). The output from the pressure transducers, load cells, and LVDTs were recorded on magnetic discs through an HP 86 micro computer and an HP 3497A Data Acquisition/Control Unit. The required computer programs were developed for subsequent plotting and analysis of data. The major computer programs are listed in the Appendix.

3.3. Soil properties

The soil used was commercially available dry coarse sillica sand with a maximum dry density of 1,570 kg/m^3, a minimum dry density of 1,340 kg/m^3 and uniformity coefficient of 1.4. The sand bed used in the tests had a density of 1,510 kg/m^3, a density index of 0.77, and an internal angle of friction of 41.2^o. The mechanical properties of the soil are listed in Table 6. The grain size distribution is shown in Figure 14. The shear strength of the soil was determined by direct shear tests and triaxial tests. The results are shown in Figures 15 and 16 and summarized in Table 6.

In order to obtain reproducible laboratory samples of the soil, the test bed

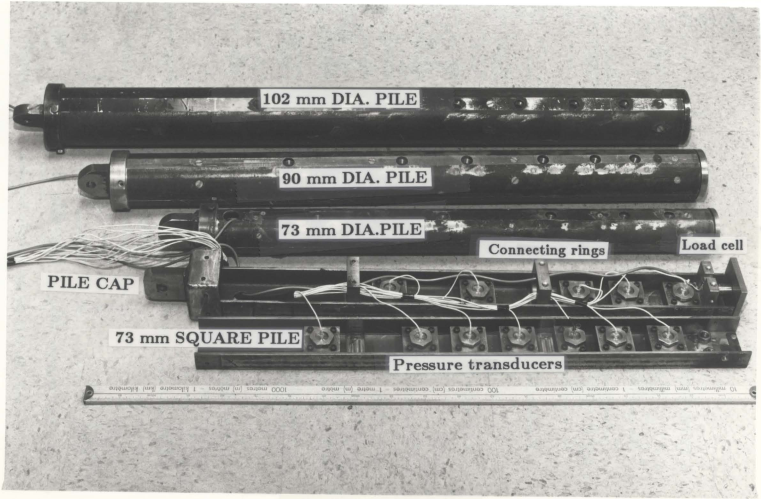

Figure 10: Model piles

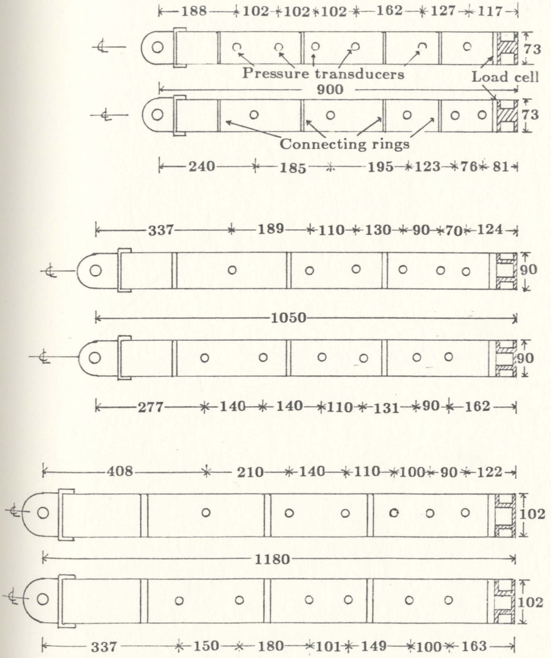

Figure 11: Details and dimensions (in mm) of piles

TABLE 4

Specification of model piles

PARAMETER	CIRCULAR PILE			SQUARE PILE
Pile width, B (mm)	73	90	102	73
Length, L (mm)	900	1050	1180	900
Thickness, t (mm)	5.3	6.1	6.0	C 75 x 40
Moment of inertia, I (m^4)	6.49×10^{-7}	1.42×10^{-6}	2.09×10^{-6}	1.01×10^{-6}
Elastic modulus, E (GPa)	200	200	200	200
Hor. coeff. of subgrade reaction for dense sand, n_h, (MN/m^3)	20	20	20	20
Max. embedded length for a short pile, L (mm)	730	854	922	798
Embedded length, D (mm)	730	800	900	730

TABLE 5

Specification of pressure transducers

PARAMETER	MODEL	
Rated pressure	3500 kPa	1750 kPa
Max. pressure	7000 kPa	3500 kPa
Rated excitation	10 V/DC	10 V/DC
Max. excitation	12 V/DC	12 V/DC
Sensitivity	0.028 mV/kPa	0.056 mV/kPa
Full scale output(FSO)	100 mV	100 mV
Thermal sensitivity	2 % FSO/ 55°c	2 % FSO/ 55°c
Comp. temperature	27°c to 80°c	27°c to 80°c
Diameter	19 mm	19 mm

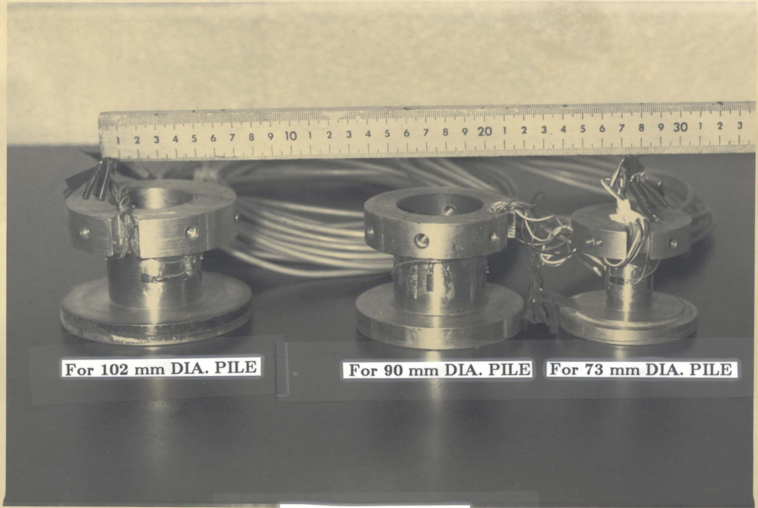

Figure 12: Load cells

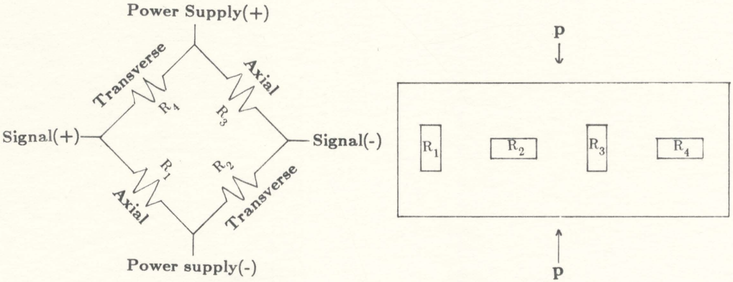

<CIRCUIT> <DEVELOPED SURFACE WITH GAUGES>

Figure 13: Strain gauge assembly for load cells

TABLE 6

Properties of the soil used

PARAMETER	QUANITY
Maximum dry density, $\rho_{d(max)}$	1570 kg/m^3
Minimum dry density, $\rho_{d(min)}$	1340 kg/m^3
Apparent density, ρ	1510 kg/m^3
Density index, I_D	77 %
Apparent angle of internal friction, ϕ	41.2°
Effective grain size, D_{10}	1.45 mm
Uniformity coefficient, Cu	1.4
Relative density, D_R	2.64
Water content, ω	0.02 %

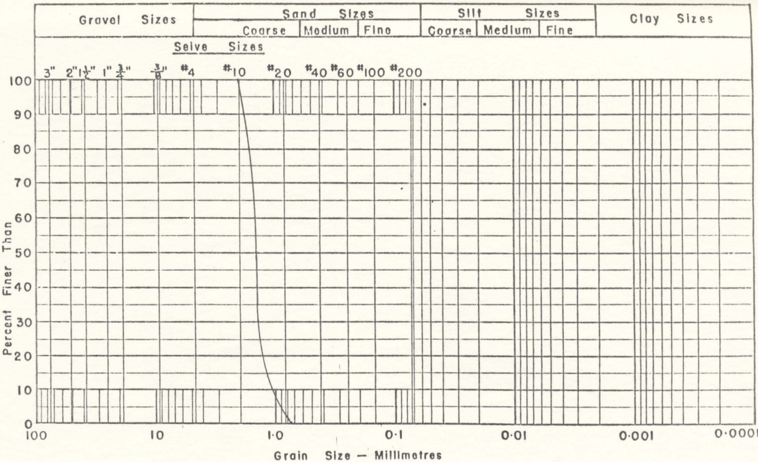

Figure 14: Grain size curve

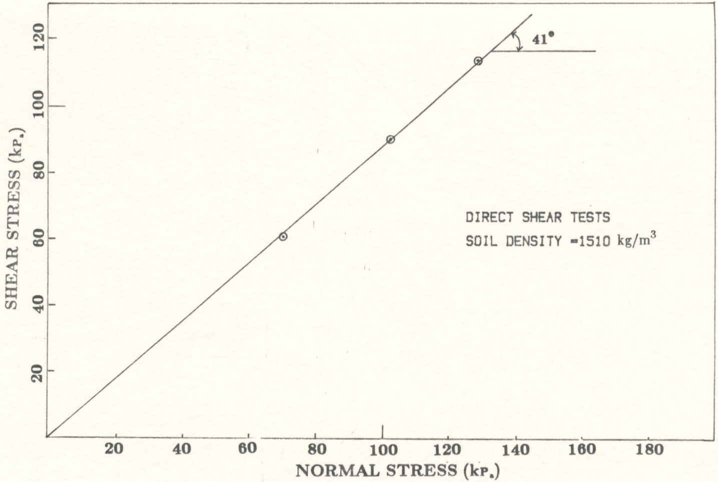

Figure 15: Results of direct shear tests

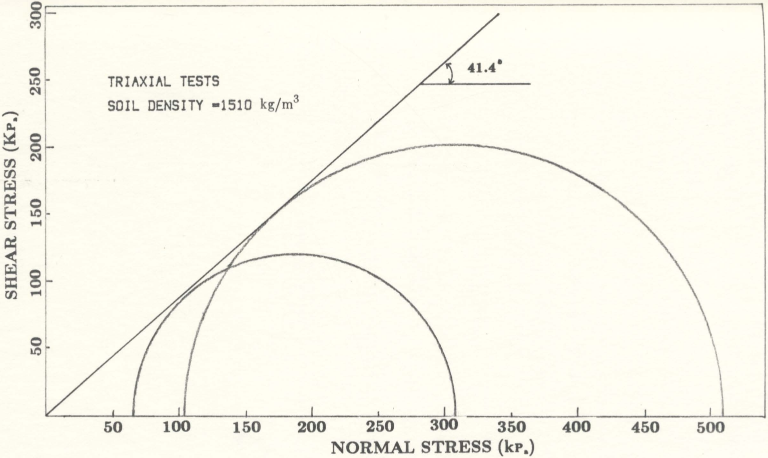

Figure 16: Results of triaxial tests

was prepared by the raining technique using a hopper shown in Figure 17. The sand was allowed to drop from the hopper through the flexible corrugated plastic hose (50 mm dia.) with a 38 mm diameter 510 mm long straight pipe at the open end. The free fall height of the sand was kept constant at about 100 mm and the sand was laid in layers of 25 mm thickness to obtain the desired density of sand (1,510 kg/m^3). Each hopper load of the soil was weighed every time the test sand bed was prepared and the actual density of the deposited sand was computed by measuring the height of the soil in the container by means of 4 measuring scales which were located at the ends of two perpendicular diameters on the inside. The total density of sand in the container for each pour was computed to ensure that the density was uniform. The uniformity of density over the entire depth of the soil was verified by cone penetrometer tests and also confirmed by point resistance force during pile pushing.

3.4. Test procedures

The piles were tested under vertical, lateral, and inclined loads. The inclinations were at 30, 45, and 60 degrees as shown in Figure 8. Pull out tests were also conducted for vertically loaded piles after the completion of the axial testing.

The following is the general procedure adopted for all the above tests in the preparation of the sand bed, loading, and data logging.

First, the test sand bed was prepared by the raining technique described earlier. The density of the sand bed for each pour was checked. If the density of soil was less than 1,500 kg/m^3 or more than 1,520 kg/m^3, the test was abandoned and a new test bed was prepared.

After the soil was placed and the density was determined to be within the acceptable range, the recording equipment was checked using the computer program to be used. The pile and the 178 kN screw jack were mounted and made ready for pushing the pile as shown in Figure 6. The pile was lowered to touch the soil. The recording equipment was rechecked manually using the data acquisition unit.

The test pile was then pushed into sand vertically in 50 mm increments at a speed of 0.8 mm/s using the manually operated 178 kN screw jack. At each 50 mm increment, the pile penetration was stopped for about 3 seconds to let the soil and equipment stabilize before readings were taken. Then 10 readings were taken on each reading device, averaged, and recorded on a magnetic disc. Penetration was then continued to the next predetermined depth up to the final depth.

After the test pile was pushed to the predetermined depth, for axial loading tests the load was removed and then reapplied measuring vertical displacements of pile by counting the number of turns of the screw jack crank, while for the inclined and horizontal load tests the 178 kN screw jack was removed and the 44.5 kN screw jack with a swivel joint was installed and set for desired inclination (30, 45, 60, and 90 degrees) as shown in Figure 7. Two LVDTs and dial gauges with a precision of 0.001 mm/div. were mounted to measure displacements of pile in the horizontal direction and the direction of the load as shown in Figure 18.

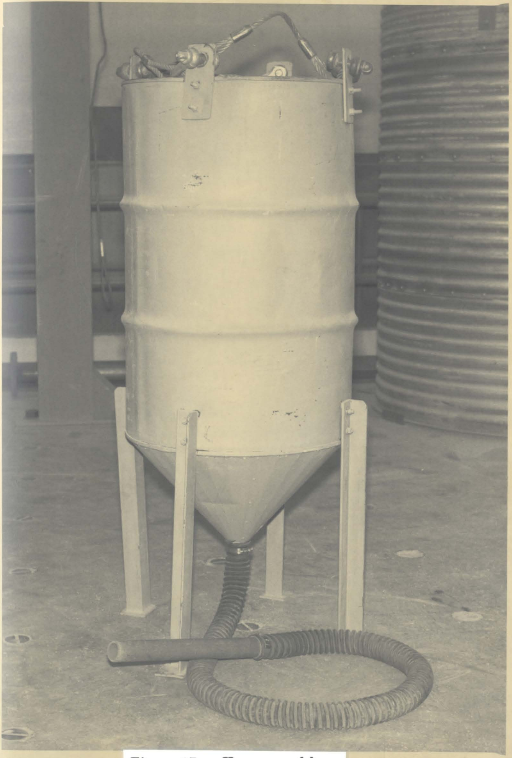

Figure 17: Hopper and hose

Figure 18: General experimental set up for inclined loads

The load was then applied from 0 to the failure load at a strain rate of about 0.2 mm/s. Data from the pressure transducers, load cells, and LVDTs were sampled, averaged, and recorded in a similar fashion to that described earlier. The test was terminated either based on the load-settlement curve or at a displacement corresponding to half the diameter of the pile.

Before removing the sand or after pushing the pile into the sand, the density of the test sand bed was periodically verified using the Fugro-type cone penetrometer; care was taken to perform the test beyond the zone of the densification influence around the pile. The cone penetrometer was pushed into the sand in increments of 50 mm at a rate of 0.8 mm/s using the 178 kN screw jack. The cone resistance was recorded using the data acquisition unit.

Pull out tests were performed on the vertically loaded piles to find the ultimate pull out resistance.

At the end of the test, the sand was removed from the soil container by opening the doors on the side of the container.

The results of the tests are presented and discussed in the following chapter along with the various theoretical predictions where such theories are available.

Chapter 4

TEST RESULTS and DISCUSSION

4.1. General

The test results and discussion have been organized under the following broad categories:

(1) Evaluation of the sand bed preparation, uniformity of test conditions, and cone penetration tests.

(2) Axial loading of the piles, evaluation of N_q, and pull out resistance.

(3) Lateral loading of piles, ultimate lateral loads, and comparison with various theoretical predictions.

(4) Piles under inclined loads, evaluation of the end resistance, and correlation with theoretical calculations.

The interrelation between the above different loading conditions is discussed at the end of the chapter.

4.2. Cone penetration tests and uniformity of test conditions

In order to obtain reproducible test conditions, the raining technique described earlier was used for the preparation of the sand bed. Densities were computed for each hopper load deposited into the container and the density achieved was 1510 $\pm$ 10 kg/m^3 for all tests. A further verification was made of the uniformity of the test bed using the static Fugro type cone penetrometer.

Figure 19a shows the variation of the static cone pressure with depth for five different tests. It may be observed that the results are scattered within $\pm$6%. The cone pressure increases linearly, and the soil sample prepared is consistently uniform.

In the bearing capacity formulation for pile foundations in sand, the point resistance force is given by Equation (3) in the form;

$$q_p = \gamma \, D \, N_q \tag{3}$$

where q_p is the point resistance pressure, γ is the effective unit weight of soil, D is the depth of pile foundation, and N_q is the bearing capacity factor.

However, beyond a certain critical depth (D_c) the point resistance does not increase significantly with depth and thus q_p tends to become constant. This critical depth (D_c) is generally believed to be in the range of 10 to 20 times the pile diameter (Kerisel 1964, Vesic 1970, Tavenas 1971). Parameters such as the width of the pile foundation, the density, and the type of the soil, influence the critical depth D_c. From the cone penetrometer results in Figures 19a and 19b it

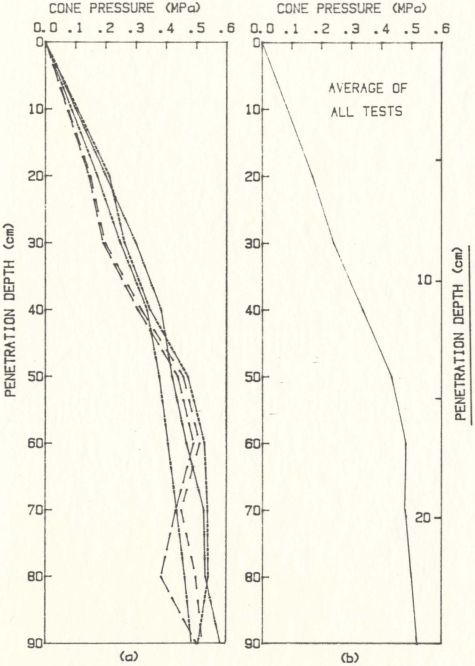

Figure 19: **The variation of cone pressure distribution with penetration depth for five typical tests**

can be seen that the cone pressure q_p tends to become constant below a depth of 16.5 times the diameter (16.5 B) which is taken as the critical depth for the soil tested.

While monitoring the cone penetration resistance, the total load on the cone penetrometer was also constantly measured at the top. The difference between the cone resistance and the total applied load was taken as the resistance due to the skin friction. The total friction as well as the unit frictional stress along the length of cone penetrometer (expressed as the average skin friction), were computed and shown in Table 7 and Figure 20. It may be seen that the frictional force also tends to reach a nearly constant value at a depth of about 19 times the diameter. The frictional stress was also measured by the friction sleeve of the penetrometer. The variation of the unit sleeve friction with depth is shown in Figure 21. It may be seen in Figure 21b that there is a reasonably good correlation between the total skin friction computed from sleeve measurement and that obtained from the measured total force on the penetrometer.

Cone penetration tests show that the soil sample was uniform and repeatable test conditions were obtained for each tests.

4.3. Axial load tests on model piles

The tests on the model piles are classified under three broad categories. In the first category discussed in this section, the pile was axially loaded to its ultimate bearing capacity and was also subsequently subjected to pull out tests.

Soon after the test bed was prepared, the pile was pushed into the sand

TABLE 7

The averaged results of five typical cone penetrometer tests given in Figure 19

DEPTH (cm)	Q_T (N)	Q_P (N)	Q_T-Q_P=Q_s (N)	q_p (kPa)	q_s (kPa)
20	171	163	8	163	0.7
30	254	242	12	242	0.72
40	347	326	21	326	0.94
50	467	432	35	432	1.24
60	523	481	42	481	1.26
70	529	478	51	478	1.3
80	555	504	51	504	1.12
90	560	502	58	502	1.14

$q_p=Q_p/A_s$

$q_s=Q_s/(0.5xA_s)$ at a given depth above critical depth

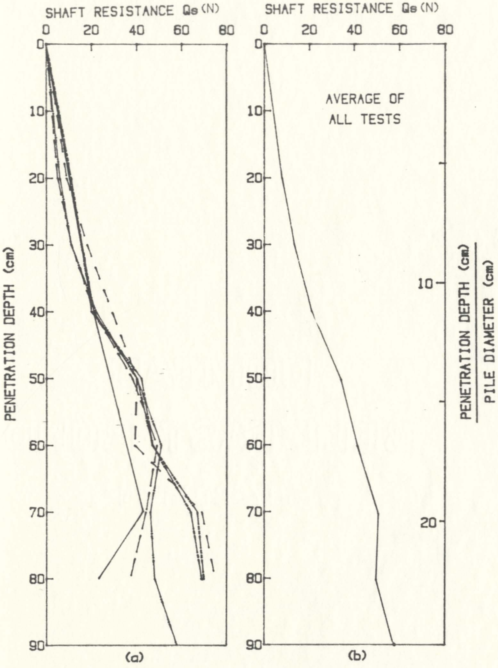

Figure 20: **The variation of shaft resistance with penetration depth for six typical cone penetrometer tests**

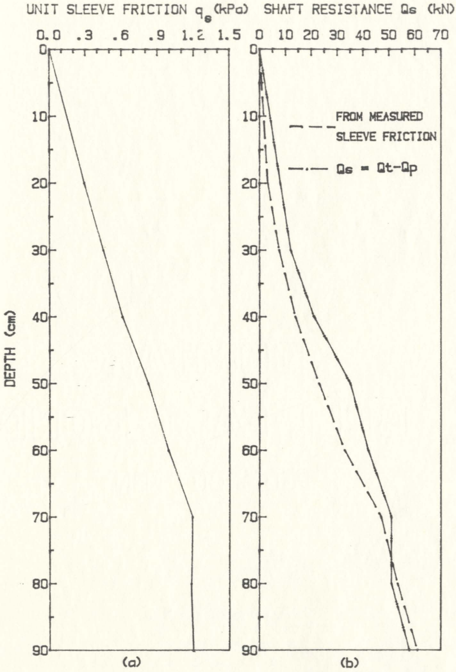

Figure 21: **The averaged variation of unit sleeve friction and shaft resistance with penetration depth**

slowly at 0.8 mm/s to the predetermined depth. Once the desired depth of foundation was reached, the load was removed and the pile was allowed to set.

The total resistance of the pile to penetration was measured by the load cell on the top of the pile, while the end resistance was measured by the load cell at the tip. The difference between the two is the shaft resistance due to skin friction. Typical results of the point resistance as the pile penetrated the soil are given in Figures 22, 23, and 24 for the piles of 73 mm, 90 mm, and 102 mm diameters respectively. The results for the three different piles are compared in Figure 25. The average unit cone resistance obtained from the cone penetrometer tests are also shown in this Figure.

From the cone penetrometer tests the critical depth for q_p for this material was found to be 16.5 times the diameter of the pile. For a 73 mm diameter pile the critical depth will therefore be in the order of 1.2 m. However, the maximum depth of penetration for the model piles was 90 cm which is less than the critical depth. It can be seen in Figure 25 that while the critical depth was reached for the cone penetrometer, the pile penetration is still less than the critical depth for all the three piles.

4.3.1. Load tests, Base resistance, and N_q

Load tests on pile foundations fall under two broad categories. In the load-controlled method, the load is applied in increments of the design load and maintained until the settlement ceases. In the displacement-controlled mode, small increments of settlement are imposed and maintained until the load reaches

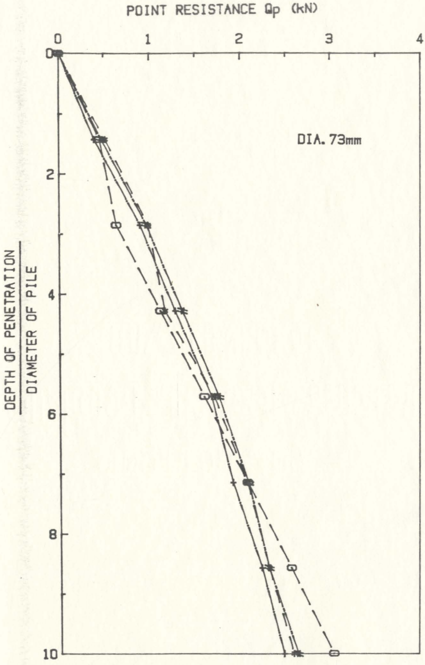

Figure 22: The variation of point resistance with relative depth (73 mm diameter)

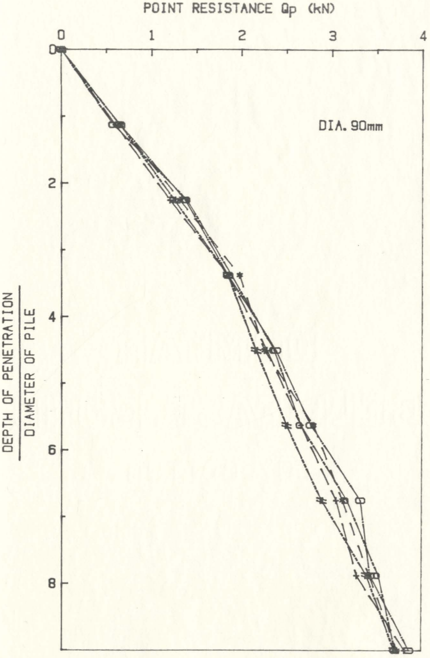

Figure 23: The variation of point resistance with relative depth (90 mm diameter)

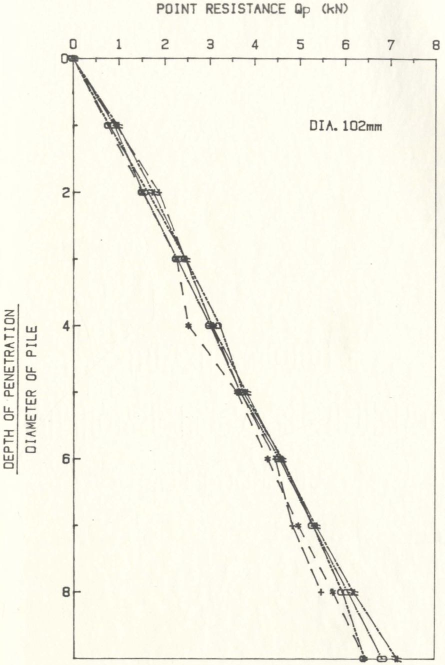

Figure 24: The variation of point resistance with relative depth (102 mm diameter)

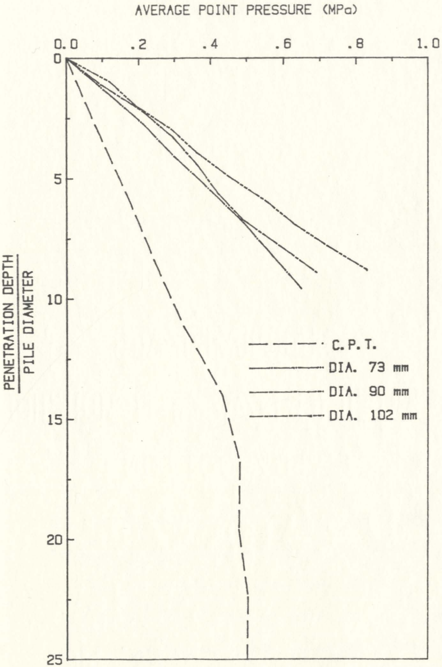

Figure 25: A comparison of average point pressure for model piles and cone penetrometer with relative depth

equilibrium. Although the process of initially pushing the pile to the required depth is a variety of load test under a vertical load, the rate and magnitude of loading, it is, however, to be noted that the resulting displacements are very large by normal standards for load tests. Nevertheless, the measured loads represent the ultimate axial bearing capacity at each depth during the process of pile penetration.

Load tests were conducted after the piles were pushed to the required depths and the loads were applied monotonically in the vertical, horizontal, or inclined directions, as required. In the case of axially loaded vertical piles, these load tests supplement the information already obtained while pushing the piles into the soil. In the case of piles under inclined and lateral loads, load tests were necessary to evaluate the ultimate load in the required direction.

The load-settlement curves for the axially loaded vertical piles are shown in Figure 26. The three sizes, 73 mm, 90 mm, and 102 mm were first pushed to a depth such that the D/B ratio was about 10 in each case. In addition, the 102 mm diameter pile alone was tested at three different D/B ratios and those load-settlement curves are shown in Figure 27. The criterion for establishing the ultimate load from load-settlement diagrams has been discussed by Whitaker (1957, 1963), Berezantzev (1965), Vesic (1967), and Poulos and Davis (1980). The point where the portion of the load-settlement curve becomes straight or substantially straight is generally taken as the failure load. These are so identified in Figures 26, and 27. It is, however, to noted that a consistent and reliable interpretation of the test results requires some familiarity, experience, and judgement.

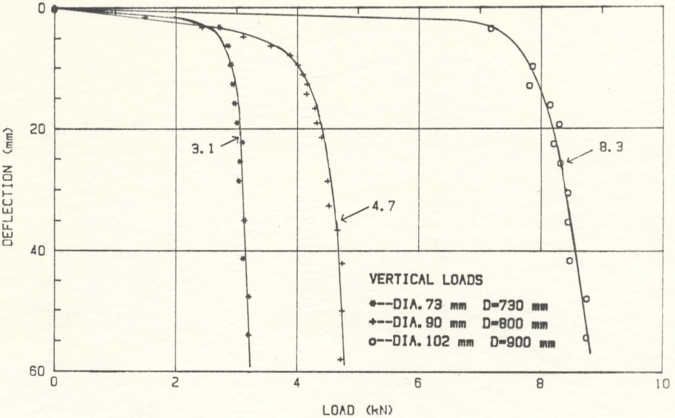

Figure 26: Load-settlement curves for model piles under vertical loads

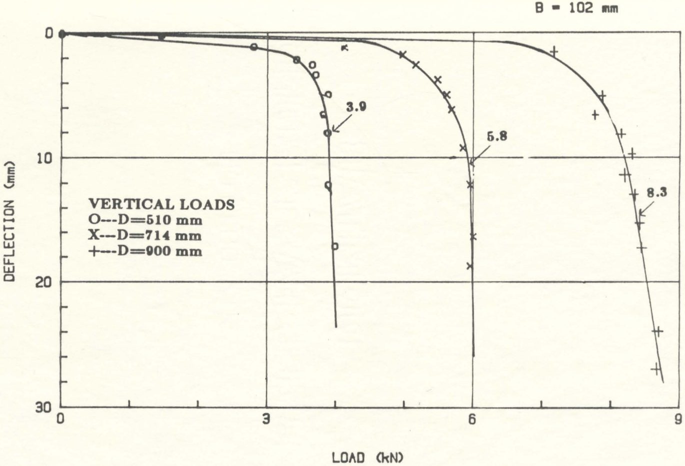

Figure 27: The load-settlement curves for a 102 mm diameter pile under vertical loads

The various theories available to determine the end bearing capacity were described in Chapter 2. The theories of Terzaghi (1943), Brinch Hansen (1951), Berezantzev (1961), Durgunoglu and Mitchell (1973), Meyerhof (1976), and Vesic(1977) were used to compute the end bearing resistance. The theoretical and experimental results are tabulated in Table 8 and also compared in Figures 28, 29, and 30 for the piles of 73 mm, 90 mm, and 102 mm diameters. The general equation for the end bearing resistance is given by;

$$q_p = \gamma \, D \, N_q \tag{3}$$

Thus for a given soil at a particular depth the end resistance depends on the assumed value of N_q. The various theories described above differ from one another in the assumed soil failure mode and hence the value of N_q varies from one theory to the other. This variation is shown in Figure 31 together with the values of N_q computed from the measured bearing capacity. It is seen that the experimental results are closest to the theoretical values of Vesic (1977). In the theoretical computation of N_q, Meyerhof (1976) suggested that the N_q increases with depth. A somewhat similar increase was suggested by Durgunoglu and Mitchell (1973) up to a certain depth while Berezantzev (1961) indicated a decrease of N_q with depth for deep foundations in sand. Vesic (1977) proposed a constant value of N_q. The variation of N_q obtained from the present tests (Figure 31) show an aggrement with the conclusions of Vesic (1977). In fact there is a slight decrease in N_q with depth.

TABLE 8

Comparison of theoretical and measured ultimate bearing loads (kN)

METHODS	PILE DIAMETER											
	73(mm)				90(mm)				102(mm)			
	D	Q_p	Q_s	Q_u	D	Q_p	Q_s	Q_u	D	Q_p	Q_s	Q_u
Terzaghi (1943)	730	5.33	0.37	5.7	800	8.89	0.54	9.4	510	7.28	0.25	7.5
									714	10.18	0.49	10.7
									900	12.84	0.78	13.6
Brinch Hansen (1951)	730	9.27	0.37	9.6	800	15.43	0.54	16.0	510	12.65	0.25	12.9
									714	17.69	0.49	18.2
									900	22.31	0.78	23.1
Berezantsev (1961)	730	7.77	0.37	8.14	800	13.02	0.54	13.6	510	10.92	0.25	11.2
									714	15.02	0.49	15.5
									900	18.2	0.78	19.6
Mitchell (1973)	730	4.30	0.37	4.7	800	7.26	0.54	7.8	510	6.11	0.25	6.4
									714	8.34	0.49	8.8
									900	10.51	0.78	11.4
Meyerhof (1976)	730	15.82	0.37	16.2	800	23.79	0.54	24.3	510	12.34	0.25	12.6
									714	22.01	0.49	22.5
									900	34.39	0.78	35.2
Vesic (1977)	730	3.62	0.37	4.0	800	6.02	0.54	6.6	510	4.94	0.25	5.2
									714	6.90	0.49	7.4
									900	8.71	0.78	9.5
Experiment	730	2.9	0.2	3.1	800	4.0	0.7	4.7	510	3.3	0.6	3.9
									714	5.0	0.8	5.8
									900	7.4	0.9	8.3

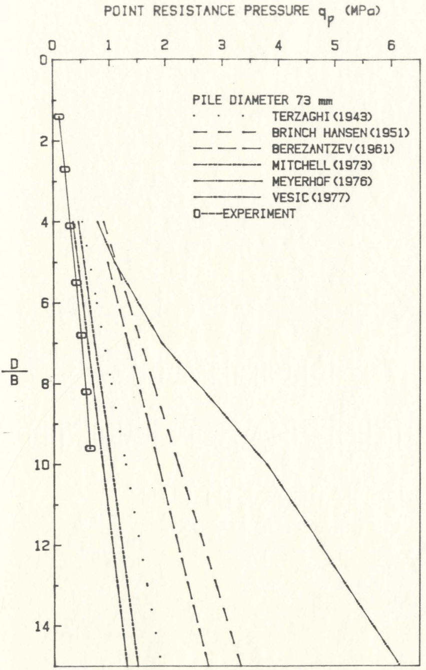

Figure 28: **A comparison of theoretical and experimental point resistance pressures with relative depth for a 73 mm diameter pile**

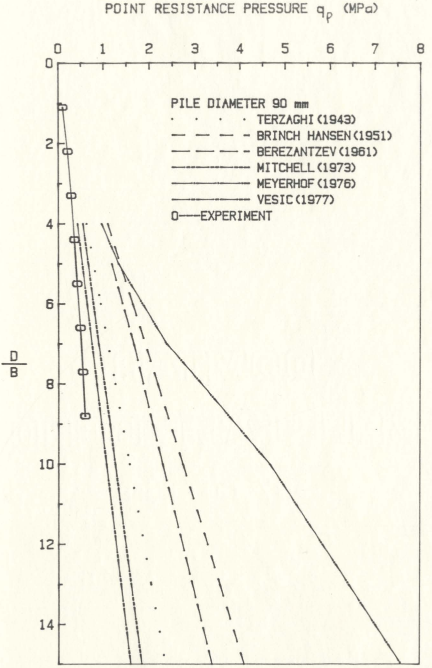

Figure 29: **A comparison of theoretical and experimental point resistance pressures with relative depth for a 90 mm diameter pile**

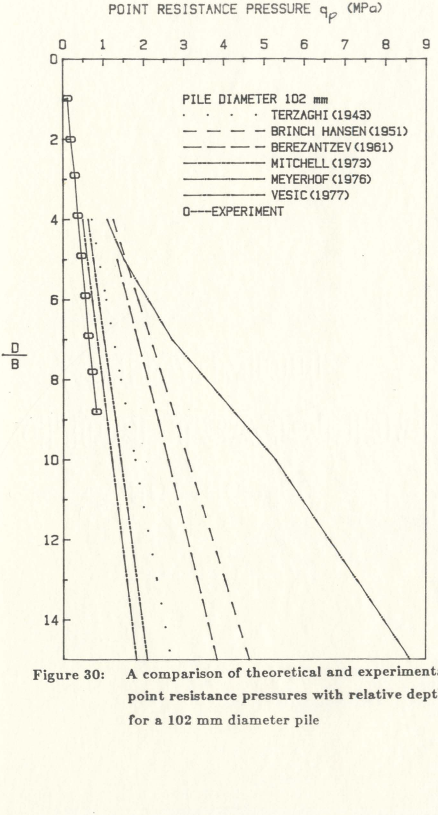

Figure 30: **A comparison of theoretical and experimental point resistance pressures with relative depth for a 102 mm diameter pile**

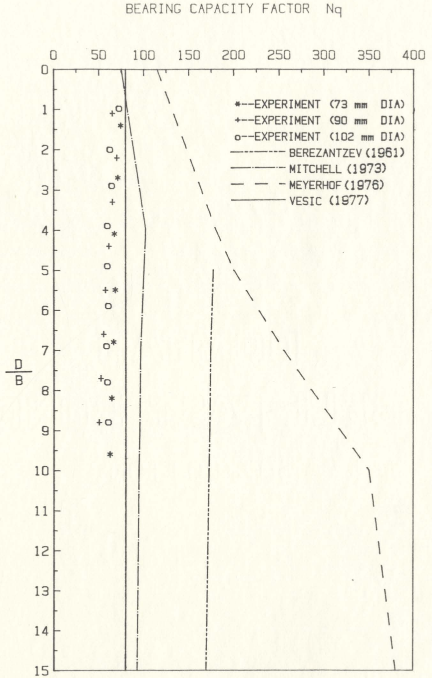

Figure 31: **The variation of bearing capacity factor N_q with relative depth**

4.3.2. Skin friction

The ultimate bearing capacity of a pile is the sum of the point (base) resistance force and the shaft friction. The point resistance force which is the primary component in cohesionless soils was discussed in the preceeding section. The averaged values of the point and shaft resistance, during pile penetration, are shown in Table 9 and Figure 32. The shaft resistance is in the order of 5 - 12% of the total ultimate resistance and can be considered as not significant, consistent with the normal practice for piles in cohesionless soils. However, during the review of the fairly extensive literature on shaft friction of piles, it was observed that there are still several uncertainties in the computation of the frictional resistance. Although the evaluation of skin friction is not a major topic in this research, some of the problems in the determination of the shaft resistance will be briefly discussed below.

The shaft resistance of a pile in sand is given by

$$Q_s = q_s A_s \tag{26}$$

where A_s is the area of the pile shaft and q_s is the unit shaft resistance.

$$q_s = q_n \tan \delta \tag{27}$$

where q_n is the normal stress acting on the foundation shaft and δ is the angle of friction between the pile material and soil.

$$q_n = K_s q_v \tag{28}$$

TABLE 9

Values of measured point resistance force and shaft resistance

DEPTH (cm)	PILE DIAMETER								
	73 mm			90 mm			102 mm		
	Q_T (kN)	Q_p (kN)	Q_s (kN)	Q_T (kN)	Q_p (kN)	Q_s (kN)	Q_T (kN)	Q_p (kN)	Q_s (kN)
20	0.92	0.88	0.04	1.18	1.08	0.10	1.71	1.63	0.08
30	1.31	1.24	0.07	1.85	1.70	0.15	2.44	2.31	0.13
40	1.84	1.70	0.14	2.28	2.13	0.15	3.15	2.96	0.19
50	2.27	2.05	0.22	2.82	2.60	0.22	3.97	3.70	0.27
60	2.61	2.37	0.24	3.37	3.08	0.29	4.91	4.50	0.46
70	3.00	2.70	0.30	3.75	3.38	0.37	5.75	5.15	0.60
80				4.28	3.74	0.54	6.51	5.90	0.61
90							7.32	6.61	0.71

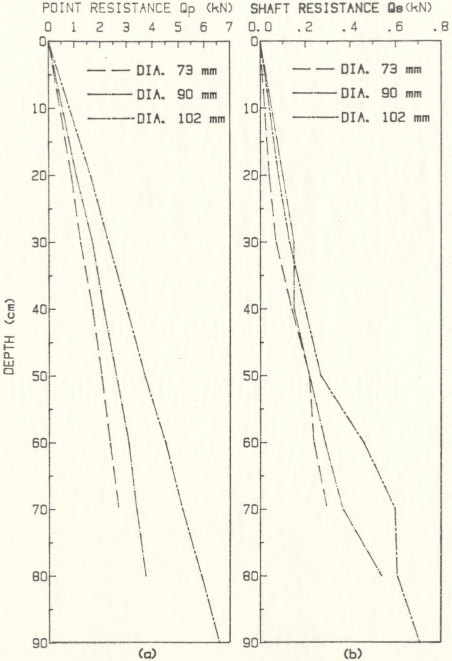

Figure 32: The variation of point resistance and shaft resistance with depth

where K_s is the coefficient of earth pressure and q_v is the effective vertical ground stress.

The computation of q_n is not simple. The coefficient of skin friction K_s is not uniform and varies with depth from the passive to active pressure range (Coyle et al. 1979). The effective ground stress reaches a critical value due to arching action. Vesic (1977) has suggested several theoretical load transfer models for evaluating Q_s, but no experimental work appears to have been conducted to verify any of those models. Cone penetrometer tests show that the shaft resistance Q_s reaches a constant value (Figure 21) somewhat similar to the critical value for the point resistance force Q_p. Even if the shaft resistance may be a fraction of the base resistance, the possibility that it could reach a critical value has to be examined as a separate research topic.

4.3.3. Pull out resistance

The pull out resistance of piles is an important parameter in the design of offshore structures. Determination of the pull out resistance of a vertical pile is also generally important in the design of tall structures against overturning moments, buoyant structures against uplift forces, and structures against frost expansion of soil, etc.

Although the resistance to pull out is the result of soil-pile friction, the pull out resistance generally tends to be less than the shaft friction discussed in the previous section. Pull out tests were conducted on the piles and load-deflection curves similar to the load tests discussed for the downward loads were obtained. The results are shown in Figure 33 and the pull out loads are identified.

Several theories have been proposed to compute the pull out resistance of piles in sand (Meyerhof 1973, Poulos 1980, Levacher and Sieffert 1984). Table 10 shows the computed pull out resistance, measured shaft friction, and measured pull out resistance. It is seen that there is a considerable variation between the measured and the computed pull out resistance. A comparison of the measured shaft friction and pull out resistance shows that a good correlation can be obtained by expressing the pull out resistance Q_s' as:

$$Q_s' = 0.5\, Q_s + W \tag{29}$$

where W is the weight of pile.

The correlation of the results using the above expression with the measured values is also shown in Table 10.

Axial loading of vertical piles shows that the existing theories generally overestimate the bearing capacity of piles in sand. Tests indicate that the shaft resistance also tends to reach a critical value similar to the end bearing resistance. This has to be investigated in some detail. The pull out resistance at the soil-pile interface is about one half of the shaft resistance.

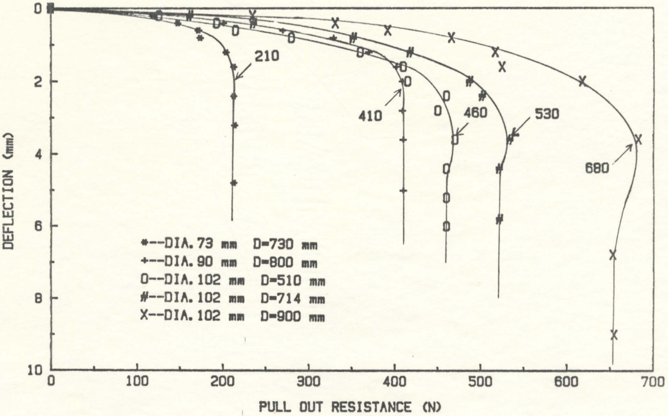

Figure 33: Load test curves for piles subjected to pull out forces

TABLE 10

Pull out resistance (kN)

PILE DIA.	D/B	Q_s	W	THEORY				EXPERIMENT	
				1	2	3	4	Q_u-Q_p	Meas.
73 mm	10	0.37	0.12	0.36	3.28	0.2	0.31	0.2	0.21
90 mm	9	0.54	0.18	0.54	4.4	0.3	0.45	0.7	0.41
102 mm	5	0.25	0.27	0.44	2.21	0.32	0.40	0.6	0.46
102 mm	7	0.49	0.27	0.6	4.08	0.38	0.52	0.8	0.53
102 mm	9	0.78	0.27	0.79	6.32	0.44	0.66	0.9	0.68

$Q_s = 0.5\ K\gamma D \tan \delta\ A_s$

1,POULOS $[(2/3)Q_s + w]$

2,MEYERHOF $[B\ \gamma\ D^2\ k_b/2 + W]$(for rough piles)

3,LEVACHER $[0.5\ K_o\gamma P \bar{h}^2 K_{mo}]$

4,PROPOSED $[Q_s/2 + w]$

W = the weight of pile

4.4. Vertical pile under lateral loads

The second series of load tests consisted of a vertical pile subjected to horizontal loads at the top of the pile. Initially the piles were pushed into the sand as described in Chapter 3. The larger screw jack was then removed and the smaller screw jack with a swivel joint was mounted on the frame and set for horizontal loads. The horizontal deflection of the pile was measured by gradually increasing lateral loads. Load-deflection curves similar to that already described were obtained. Typical curves for the piles of 73 mm, 90 mm, and 102 mm diameters are shown in Figures 34, 35, and 36. The ultimate lateral resistance of each pile was obtained as already described, from the load-deflection curves.

The theoretical lateral load capacity of a circular pile can also be obtained considering the pressure distribution along the length of the pile. The formulations developed by Brinch Hansen (1961), Broms (1961), Petrasovits and Adams (1972), and Meyerhof et al. (1976, 1981) can be used to find the total lateral soil resistance. The details of these theories were discussed in Chapter 2. All the above theories take into account the effect of eccentricity e, which is the distance between the point of application of load and the soil surface. As the value of e becomes greater relative to the pile length below the ground level, there is a corresponding reduction in the ultimate lateral capacity. This effect is shown in Figures 37, 38, and 39 for the various theories and for the different pile diameters. The measured value of the ultimate lateral load is also shown in these figures. It may be seen that the values predicted by all theoretical methods are higher than the measured values. Meyerhof's (1981) theory is the closest to the

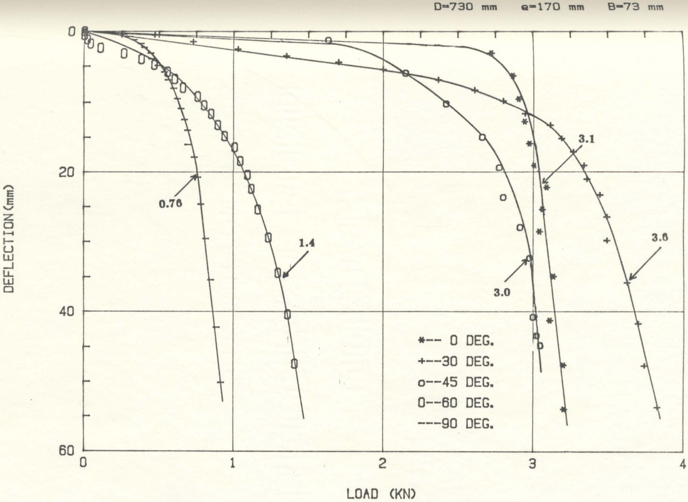

Figure 34: Load- curves for a 73 mm diameter pile under inclined loads

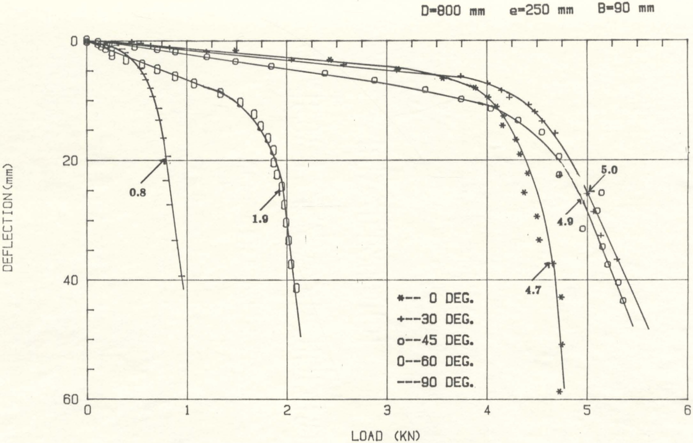

Figure 35: Load-deflection curves for a 90 mm diameter pile under inclined loads

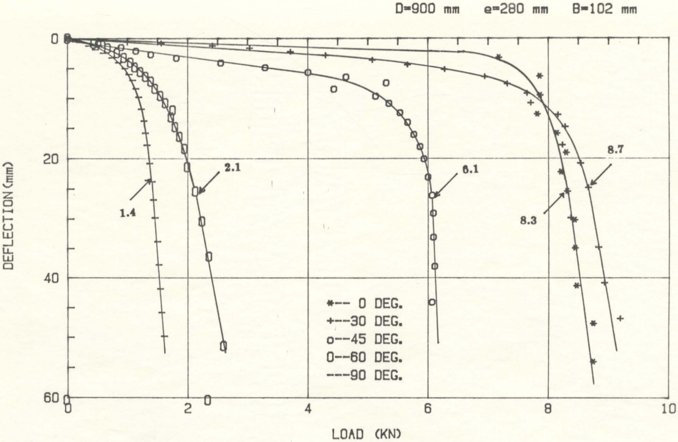

Figure 36: Load-deflection curves for a 102 mm diameter pile under inclined loads

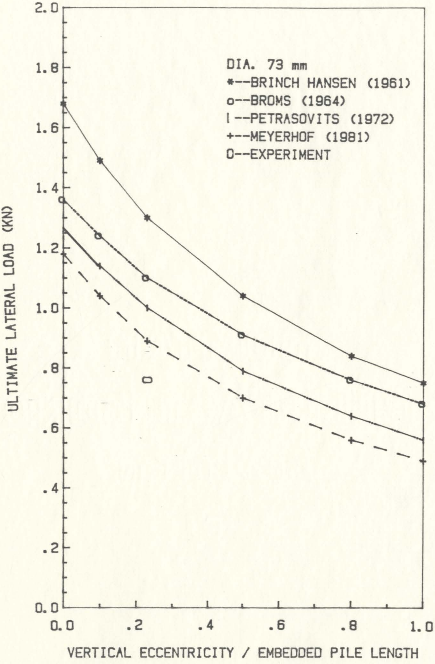

Figure 37: The variation of ultimate lateral load with the ratio e/D for a 73 mm diameter pile

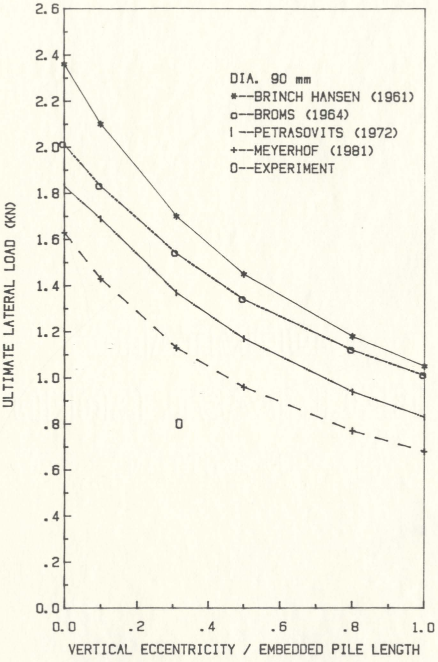

Figure 38: **The variation of ultimate lateral load with the ratio e/D for a 90 mm diameter pile**

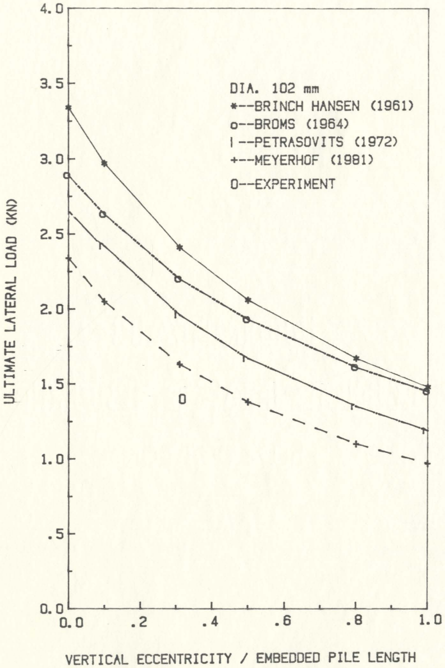

Figure 39: The variation of ultimate lateral load with the ratio e/D for a 102 mm diameter pile

experimental values. In all the above theories, it is assumed that the pressure acts uniformly on the projected width of the pile which for a circular pile is its diameter. If p is the pressure at any point, the lateral force Q_n is given by

$$Q_n = \sum_{x=o}^{D} p_x B$$

$$= \int_{x=0}^{D} p_x B \, dx \qquad (30)$$

where B is the pile diameter.

A nomenclature diagram explaining the above concept is given in Figure 40.

For a circular pile, it is inappropriate to assume that the pressure will be a constant across the diameter. In fact, at the two ends, it is most probable that the pressure is zero or nearly so while at the center where the curvature is a maximum relative to the direction of the pile movement, the pressure will be a peak value. This concept is also shown in Figure 40. Pressures which are measured experimentally are these maximum pressures. Using this approach, the measured ultimate lateral loads were compared with theoretical computations as shown in Table 11. It may be seen that the measured values tend to be closer to computed values when the pressure across the pile diameter is assumed to be parabolic instead of a rectangular distribution. In order to further verify the above assumption, a 73 mm square pile was fabricated and tested under lateral loads. The load test results are shown in Figure 41 and the ultimate load is compared with that for the circular pile in Table 11. It may be seen that there is a better agreement between the various theories and the result from the square

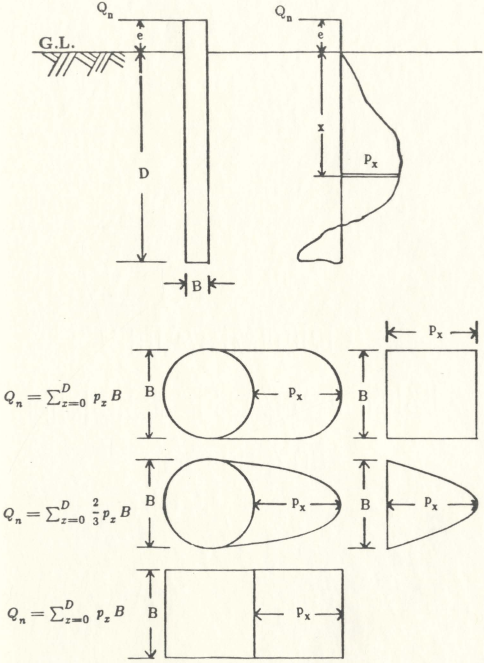

Figure 40: Lateral earth pressure distribution along the pile length and across the pile width

TABLE 11

Computed and measured ultimate lateral resistance

DIAMETER	THEORY	LATERAL RESISTANCE			
		CALCULATED		EXPERIMENTAL	
		$\sum P_x B$ (kN)	$\frac{2}{3}\sum P_x B$ (kN)	CIRCULAR (kN)	SQUARE (kN)
73 mm	Brinch Hansen	1.3	0.87	0.76	0.92
	Broms	1.1	0.73		
	Petrasovits	1	0.67		
	Meyerhof	0.89	0.59		
90 mm	Brinch Hansen	1.7	1.13	0.8	
	Broms	1.54	1.03		
	Petrasovits	1.37	0.91		
	Meyerhof	1.13	0.75		
102 mm	Brinch Hansen	2.41	1.6	1.4	
	Broms	2.2	1.47		
	Petrasovits	1.96	1.3		
	Meyerhof	1.63	1.09		

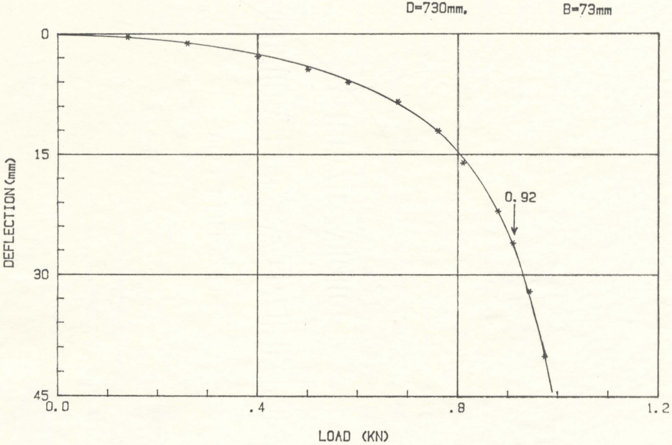

Figure 41: Load-deflection curve for a square pile of 73 mm under lateral loads

pile test. Assumption of a uniform pressure across the diameter will lead to an overestimation of the ultimate capacity of circular piles.

It is also seen from Table 11 that the computations using the theories of Broms and Petrasovits are closer to the measured lateral capacities. One of the reasons for the differing theoretical estimates between the various theories in Table 11 is the assumed pressure distribution along the length of the pile. Those pressure distributions are shown in Figures 42, 43, and 44 for the different pile diameters together with the measured pressure distribution at failure superimposed therein. It is seen that the actual pressure distribution curve is entirely different from all the theoretical assumptions. Adams and Radhakrishna (1973) reported tests on a pile under lateral loads and obtained a lateral pressure distribution somewhat similar that obtained in this work. Chari and Meyerhof (1983) have reported a similar pressure distribution. It is reasonable to conclude that the best estimate of the lateral load capacity is obtained by considering the nonlinear pressure distribution from the experimental measurement.

The soil pressure along the length of the pile at the ultimate lateral load is shown in Figures 45, 46, 47, and 48 for the different piles. A comparison is made in Table 12 between the applied lateral load and that integrated from the pressure distribution. There is a net unbalanced force in all cases which most likely acts as a reaction at the base of the pile. No definite correlation can be made with the limited data available at present, but it is suggested that this should be examined further to quantify the pressure distribution in terms of the soil properties.

Based on the soil pressure distribution, shown in Figures 45, 46, 47, and 48, the location of the point of rotation was examined. It was found that the depth of rotation D_o is not very much influenced by the magnitude of the applied load, and is located at about 0.75 D. This compares well with the results reported by Chari and Meyerhof (1983).

Pile tests under lateral loads show that the existing theories require some modifications. For circular piles, the pressure distribution across the diameter is not likely to be constant. Further work is required to quantify the reaction at the base considering the base area of a larger pile and the pressure distribution along the length of the pile.

4.5. Vertical pile under inclined loads

In the last series of tests, the behaviour of vertical piles under inclined loads was studied. Presently available data on the behaviour of piles subjected to inclined loads are somewhat limited.

The test bed was prepared similar to the other tests and the pile was pushed into the soil as described earlier. Inclined loads were applied using the small jack and the inclination of the load was facilitated by means of a swivel joint on top of the jack. The load on the pile, the lateral pressures, the end resistance at the tip of the pile, and deflections were measured as described earlier for the lateral load tests and recorded using the data logging system. The ultimate inclined load in each case was experimentally determined from load-deflection curves as already described and shown in Figures 34, 35, and 36. Figure 49 shows the results of

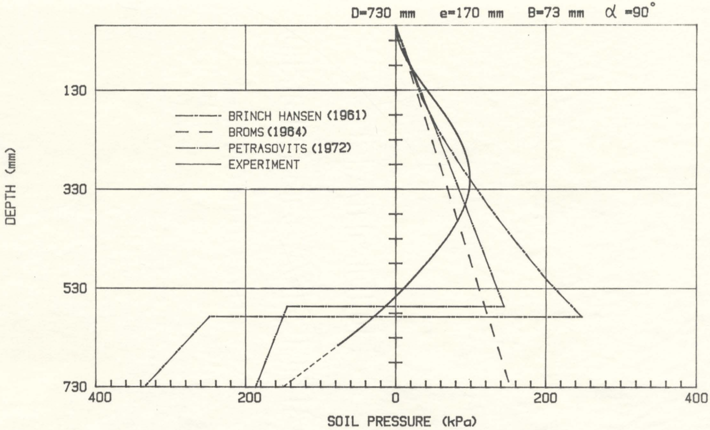

Figure 42: **A comparison of assumed and actual soil pressure distribution along the pile length under lateral loads for a 73 mm diameter pile**

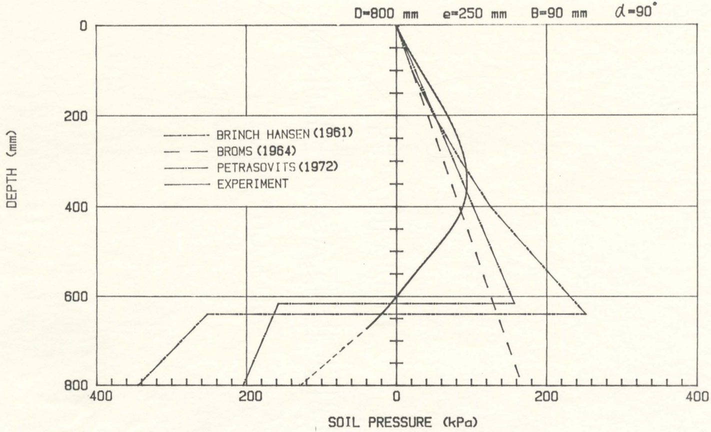

Figure 43: **A comparison of assumed and actual soil pressure distribution along the pile length under lateral loads for a 90 mm diameter pile**

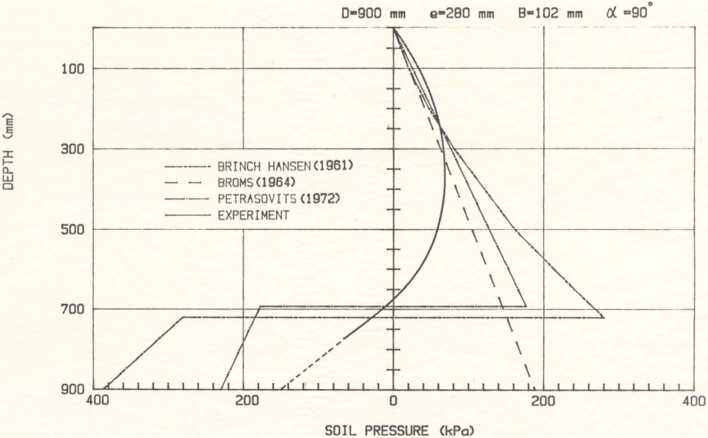

Figure 44: acomparison of assumed and actual soil pressure distribution along the pile length under lateral loads for a 102 mm diameter pile

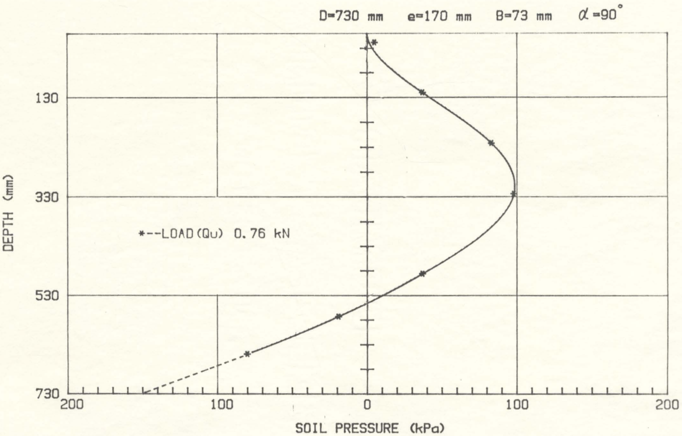

Figure 45: The measured soil pressure distribution along the length of a 73 mm diameter pile under lateral loads

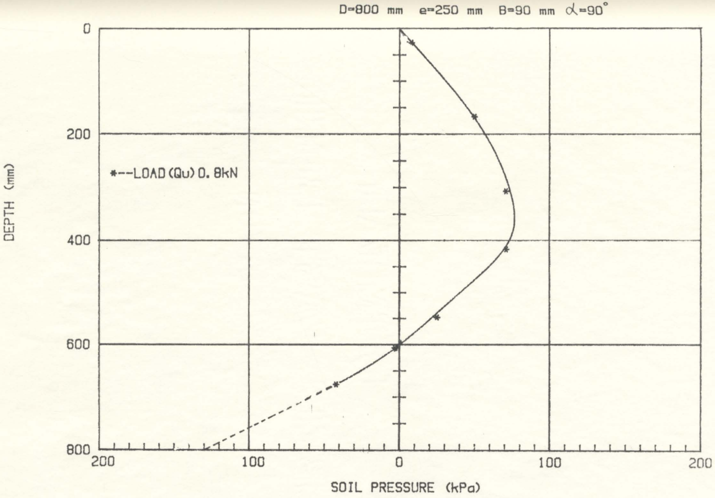

Figure 46: **The measured soil pressure distribution along the length of a 90 mm diameter pile under lateral loads**

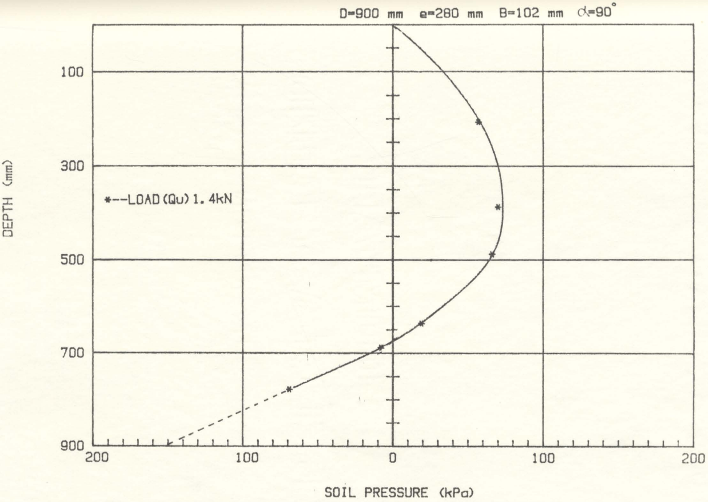

Figure 47: The measured soil pressure distribution along the length of a 102 mm diameter pile under lateral loads

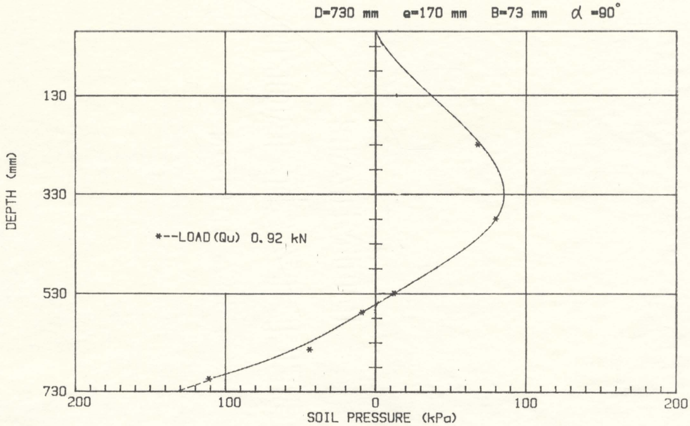

Figure 48: **The measured soil pressure distribution along the length of a square pile of 73 mm under lateral loads**

TABLE 12

Computed and measured lateral resistances based on the actual pressure distribution

CIRCULAR PILE DIA. (mm)	SQUARE PILE WIDTH (mm)	D (mm)	e/D	ASSUMPTIONS		
				Q_{hm} (kN)	Q_{hc} (kN)	R_{tip} (kN)
73		730	0.23	0.76	0.84	-0.08
90		800	0.31	0.8	0.91	-0.11
102		900	0.31	1.4	1.34	0.06
	73	730	0.23	0.92	1.21	-0.29

$Q_{hm} = Q_u$

$Q_{hc} = \frac{2}{3} B \sum P_x$ (for circular piles)

$Q_{hc} = B \sum P_x$ (for square piles)

$Q_{hc} = Q_{hm1} - Q_{hm2}$

$R_{tip} = Q_{hc} - Q_{hm}$

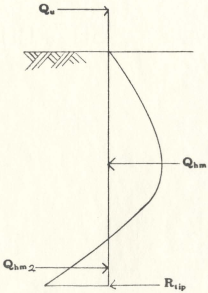

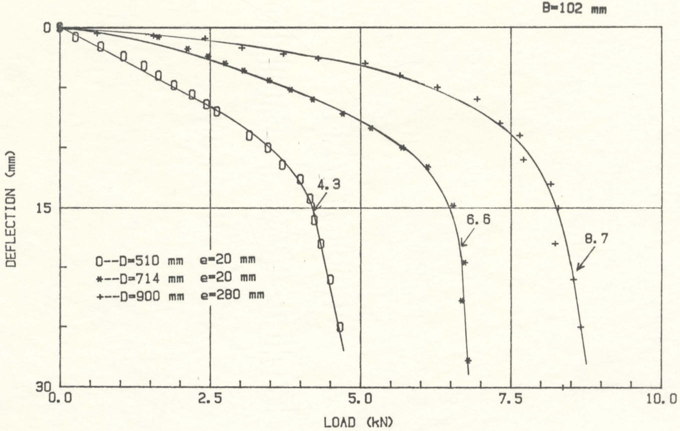

Figure 49: Load-deflection curves for a 102 mm diameter pile at 30° load inclinaion at different embedment depths

inclined load tests of a 102 mm diameter pile at 30 degrees with different embedments and eccentricities.

As already noted in an earlier section, the measured ultimate axial load capacity was closest to Vesic's (1977) theory and the ultimate lateral resistance was closest to that of Meyerhof (1981). These two theories were used to compute the ultimate axial and lateral loads. From these limiting loads and using the interaction equation of Meyerhof and Ranjan (1981), the bearing capacity at different inclinations of the load was theoretically computed and compared with the measured values. These results are shown in Figures 50, 51, and 52, and in a polar representation, in Figure 52A. It is seen that the computed results are consistently lower than the experimental values at all the load inclinations. The results are also shown in Table 13. The ultimate pile capacity under inclined loads was also computed as a percentage of ultimate vertical load capacity. The results are shown in Figure 53. It is seen that at a load inclination of 30 degrees the ultimate bearing capacity increases by 5 to 16 % compared to the vertical load capacity. It can also be seen that the ultimate bearing capacity reduces rapidly when the inclination of load is between 45 to 60 degrees. These experimental results are somewhat similar to those reported by Berezantzev et al. (1961), and Awad and Petrasovits (1968).

If Q_a is the ultimate bearing capacity under an axial load, Q_n, the ultimate lateral load capacity, and Q_u, the ultimate load at an inclination α, it may be concluded

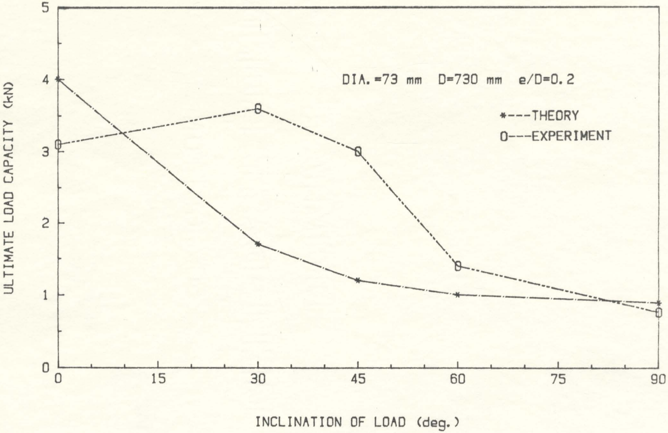

Figure 50: **A comparison of theoretical and measured ultimate load capacities with load inclination for a 73 mm diameter pile**

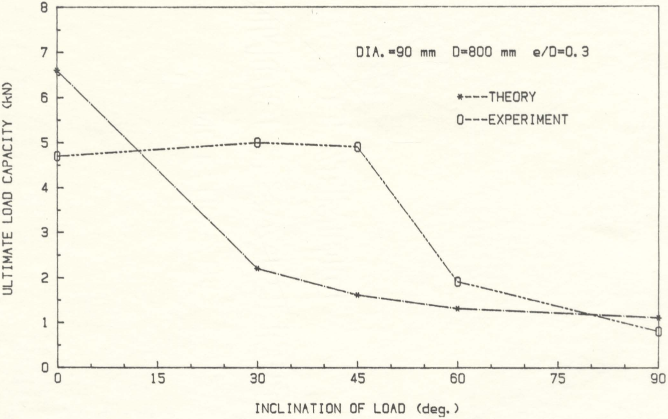

Figure 51: A comparison of theoretical and measured ultimate load capacities with load inclination for a 90 mm diameter pile

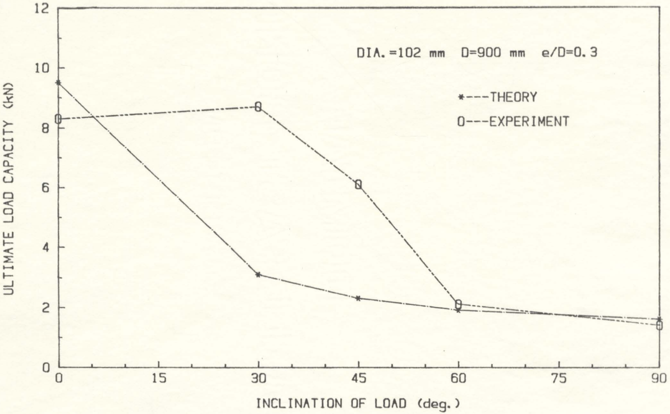

Figure 52: **A comparison of theoretical and measured ultimate load capacities with load inclination for a 102 mm diameter pile**

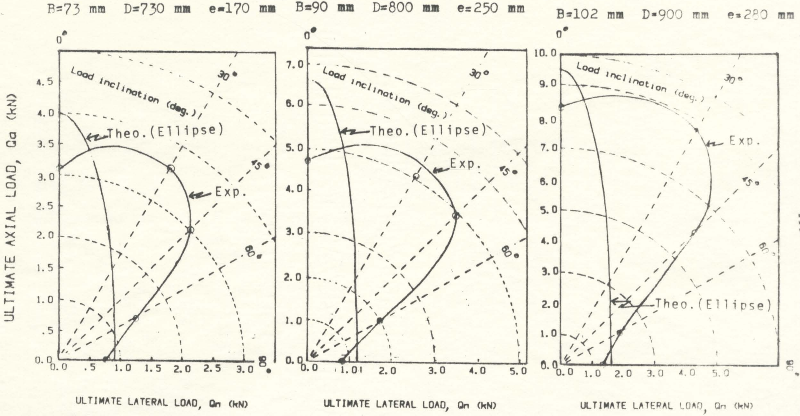

Figure 52A: The variation of ultimate bearing capacity with load inclination for model piles

TABLE 13

Theoretical bearing capacity under inclined loads

D(mm)	e/D	α(deg)	Theo.Q_u(kN)	Exp.Q_u(kN)
73	0.23	0	4.0	3.1
		30	1.7	3.6
		45	1.2	3.0
		60	1.0	1.4
		90	0.89	0.76
90	0.31	0	6.6	4.7
		30	2.2	5.0
		45	1.6	4.9
		60	1.3	1.9
		90	1.13	0.8
102	0.31	0	9.5	8.3
		30	3.1	8.7
		45	2.3	6.1
		60	1.9	2.1
		90	1.63	1.4

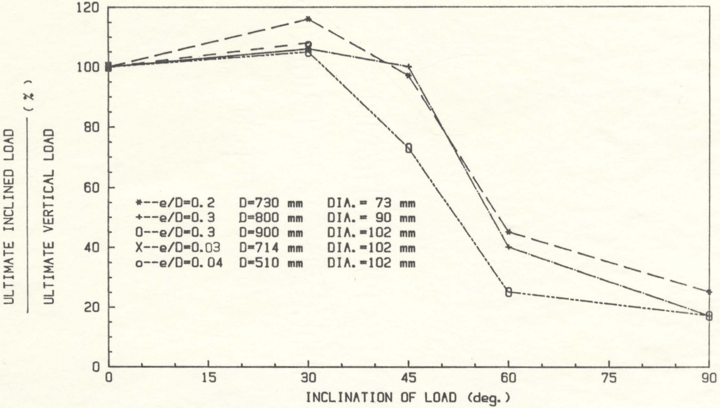

Figure 53: The variation of the ratio Q_a/Q_u with load inclination for model piles

that $Q_u \cos \alpha < Q_a$ (31)

$$Q_u \sin \alpha < Q_n \quad (32)$$

Recalling that Q_n is the lateral capacity when the pile is not under any axial load, equation (32) can be modified and expressed as

$$Q_u \sin \alpha < k\, Q_n \quad (33)$$

where k is a factor which depends on α.

From (31) and (33), Q_u can be maximized and the corresponding value of α may be expressed as

$$tan\ \alpha = \frac{k\,Q_n}{Q_u} \text{ ---------(34)}$$

The component Q_u cos α and Q_u sin α are shown in Table 14 from which the value of k may be estimated to be in the order of 3.0. Based on the simple analysis presented above the critical angle α for a maximum Q_u can be estimated. While it can be shown theoretically that the ultimate load capacity will increase with the load inclination up to an angle of 30^o - 35^o, this is a potential area of further detailed mathematical analysis and experimental study.

The variation of lateral earth pressures along the pile length under inclined loads are plotted in Figures 54, 55, and 56 for the piles of 73mm, 90 mm, and 102 mm diameters. A summary of all the tests under inclined loads is presented in Table 15. The depth of pile rotation was examined based on the earth pressure distribution and it is seen that D_0 increases initially with increasing α to about 45^{o} and then decreases as shown in Table 15. This is found to be true for all the piles. It is also noticed in this table that the end resistance under inclined loads is not likely to decrease continuously with inclination of load, and that the pile diameter has little effect on the variation of the D_0/B ratio with the load inclination.

Although some correlations can be established between the measured pressure distribution and the ultimate inclined load capacity similar to that attempted for the lateral load Q_n, it is felt that further experimental work will be necessary before any conclusions can be drawn.

Based on the test results and discussion, a set of conclusion and areas requiring further work are presented in the following chapter.

TABLE 14

Pile tests under inclined loads-components of the ultimate load

PILE DIA. (mm)	α (deg)	Q_u (kN)	$Q_u \cos\alpha$ (kN)	$Q_u \sin\alpha$ (kN)
73	30	3,6	3.1	1.8
	45	3.0	2.1	2.1
	60	1.4	0.7	1.2
	90	0.76	0	0.76
90	30	5.0	4.3	2.5
	45	4.9	3.5	3.5
	60	1.9	0.95	1.65
	90	0.8	0	0.8
102	30	8.7	7.5	4.35
	45	6.1	4.3	4.3
	60	2.1	1.05	1.8
	90	1.4	0	1.4

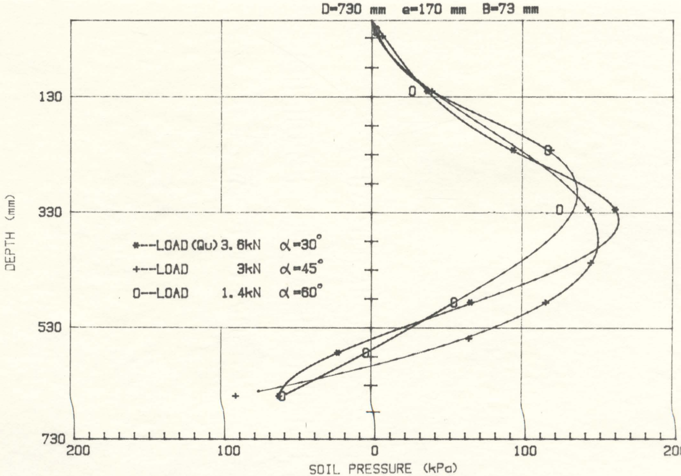

Figure 54: The measured soil pressure distribution along the length of a 73 mm diameter pile under inclined loads

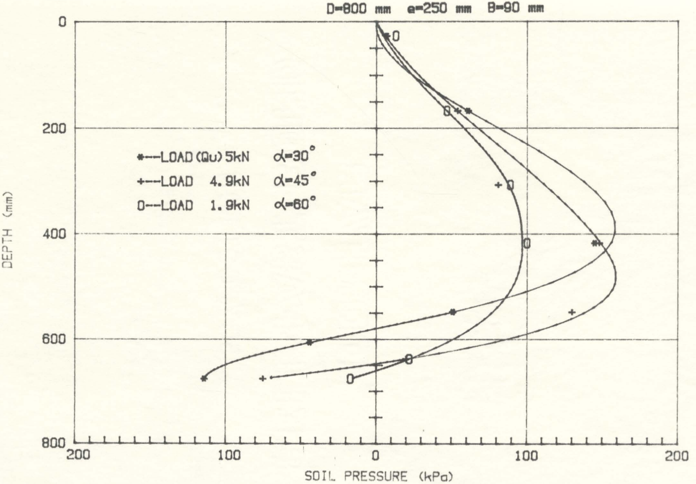

Figure 55: The measured soil pressure distribution along the length of a 90 mm diameter pile under inclined loads

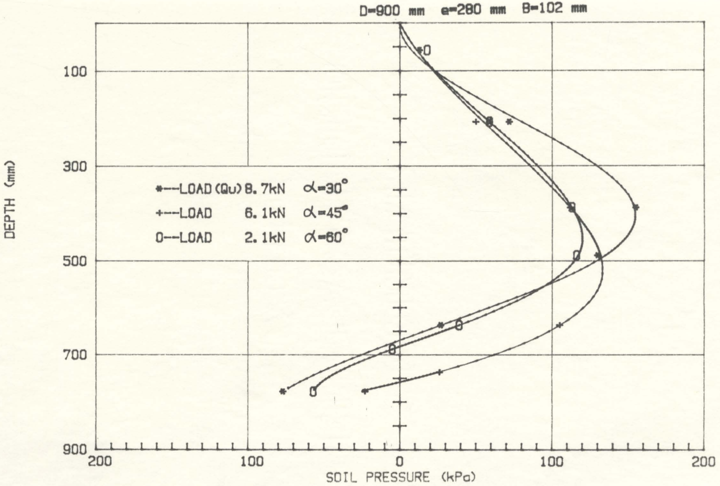

Figure 56: **The measured soil pressure distribution along the length of a 102 mm diameter pile under inclined loads**

TABLE 15

Summary of tests under inclined loads

B (mm)	D (mm)	D/B	e (mm)	e/D	α (deg)	Q_u (kN)	Q_p (kN)	D_o (mm)	β (deg)	D_o/D	D_o/B
73	730	10	170	0.23	0	3.1	2.9				
					30	3.6	3.2	549	1.88	0.75	7.5
					45	3	1.5	596	2.2	0.82	8.2
					60	1.4	0.4	568	3.0	0.78	7.8
					90	0.76	0	546	2.2	0.75	7.5
90	800	8.9	250	0.31	0	4.7	4				
					30	5.0	4.2	580	1.28	0.74	6.6
					45	4.9	3.7	647	1.56	0.8	7.1
					60	1.9	1.5	661	1.82	0.83	7.3
					90	0.8	0	600	1.81	0.75	6.7
102	900	8.8	280	0.31	0	8.3	7.4				
					30	8.7	7.7	669	1.11	0.74	6.6
					45	6.1	4.2	758	1.36	0.84	7.4
					60	2.1	1.7	682	1.85	0.76	6.7
					90	1.4	0	674	1.78	0.75	6.6

Chapter 5

SUMMARY and CONCLUSIONS

Laboratory experiments were conducted to better understand the behaviour of a vertical short rigid pile under inclined loads in sand and the comparison was made of experimental and theoretical values. The following conclusions are drawn on the results of this research work.

(1) Cone penetration tests show that fairly uniform and repeatable test conditions are obtained for the soil using the raining technique. The critical depth for the soil used was found to be 16.5 B consistent with the range of values reported in the literature.

(2) The values for the bearing capacity factor N_q, compare well with those obtained by Vesic (1977). The value of N_q does not vary with depth and is found to be nearly constant. All existing theories are found to generally overestimate the bearing capacity of piles in sand.

(3) The shaft resistance in sands is only a fraction of the total ultimate capacity. However, preliminary analysis shows that this shaft resistance also reaches a critical value. Further study is required to show how shaft resistance is affected by method of pile installation.

(4) The pressure distribution along the length of the pile is nonlinear, contrary to the assumptions made in the various existing theories. Further work is required to obtain an analytical solution to the actual pressure distribution.

(5) Pull out resistance of a vertical smooth pile is estimated as about one half of the shaft resistance; This is a modification of the presently available theoretical estimates and gives a good correlation with actual measured values.

(6) Predictions of ultimate lateral resistance for circular piles using existing theories overestimate the load capacity. This may be due to the assumption that the lateral soil pressure is uniform on the projected width of pile. For the calculation of lateral resistance of a circular pile, the shape of pressure distribution across the pile diameter is to be taken into account. A parabolic pressure distribution is suggested for better correlation.

(7) The point of rotation of the pile under lateral load was found to be about 0.75 times the embedment depth and is not much influenced by the magnitude of the applied load. This result compares well with the results reported by Chari and Meyerhof (1983).

(8) The ultimate bearing capacity of a pile under a load inclined at 30^{o} was 5 to 16 % higher than the axial ultimate bearing capacity. The ultimate bearing capacity decreases gradually after a 30^{o} inclination. The reduction is rapid for inclinations larger than 45^{o}. This result compares well with the published results by Adams and Petrasovits (1968). Further theoretical work is required to examine this phenomenon in detail.

REFERENCES

1. Adams, J. I. and Radhakrishna, H. S. (1973). "The lateral capacity of deep augered footings." 8th Int. Soc. Soil Mech. Vol. 3, Moscow, pp.1-8.

2. Awad, A. and Petrasovits, G. (1968). "Considerations on the bearing capacity of vertical and batter piles subjected to forces acting in different directions." Proc. 3rd Conf. S. M. & F. E., Budapest, pp.484-497.

3. Berezantzev, V. G., Khristoforov, V. S. and Golubkov, V. N. (1961). "Load bearing capacity and deformation of piled foundations." Proc. 5th Int. Conf. S. M. & F. E.,Vol. 2, pp.11-15.

4. Bieganousky, Wayne A. and Marcuson, William F. (1976). "Uniform placement of sand." ASCE, Vol. 102, No. GT3, pp.229-233.

5. Bjerrum, L. (1973). "Geotechnical problems involved in foundations of structures in the North Sea." Geotechnique, Vol. 23, No. 3, pp.319-358.

6. Brinch Hansen, J. (1951). "Simple statical computation of permissible pile loads." Christiani and Nielsen Post, pp.14-17.

7. Brinch Hansen, J. (1961). "The ultimate resistance of rigid piles against transversal forces." Danish Geotechnical Institute, Bul. No. 12, Copenhagen, pp.5-9.

8. Broms, Bengt B. and Silberman, Jorge O. (1964). "Skin friction resistance for piles in cohesionless soil." Sols Soils, Vol. 3, No. 10, pp.33-43.

9. Broms,Bengt B. (1964). "Lateral resistance of piles in cohesionless soils." ASCE, Vol. 90, No. SM3, pp.123-156.

10. Broms, bengt B. (1965). "Piles in cohesionless soils subject to oblique pull." ASCE, Vol. 91, No. SM4, pp.199-205.

11. Broms, Bengt b. (1966). "Methods of calculating the ultimate bearing capacity of piles, a summary." Sols Soils, No. 18-19, pp.21-31.

12. Chari, T. R. and Meyerhof, G. G. (1983). "Ultimate capacity of rigid single piles under inclined loads in sand." Can. Geotech. J., Vol. 20, pp.849-854.

13. Coyle, H. M. and Castello, R. R. (1979). "A new look at bearing capacity

factors for piles." 11^{th} Offshore Technology Conference, Huston, pp.427-435.

14. Christensen, N. H. (1961). "Model tests with transversally loaded rigid piles." Bul. No. 12, Geoteknisk Inst., Copenhagen, pp.10-16.

15. Craig, R. F. (1978). "Soil Mechanics." 2^{nd} Eddition, Van Nostrand Reinhold Co.

16. Davisson, M. T. and Prakash, Shamsher (1963). "A review of soil-pole behaviour." Highway Res. Rec. No. 39,pp.25-48.

17. Durgunoglu, H. Turan and Mitchell, James K. (1973). "Static penetration resistance of soil" Space Sciences Laboratory Series 14 Issue 24, Univ. of Cal.

18. Evans, L. T. (1953). "Bearing piles subjected to horizontal loads." ASTM. Special Tec. Publ. No. 154, pp.30-37.

19. Geocon LTD.(1969). "Laboratory tests of soil sample, Grand Banks." Report F 1103, Rexdale, Ontario.

20. Kerisel, Jean (1964). "Deep foundations basic experimental facts." Proc. of the North American Conf. on Deep Foundtion, Mexico, Vol. 1, pp.5-44.

21. Kezdi, A. (1957). "Bearing capacity of piles and pile groups." Proc. 4^{th} Int. Conf. S. M. & F. E., Vol. 2, pp.47-51.

22. Kishida, Hideaki (1963). "Stress distribution by model piles in sand." Soils and Foundations, Vol. 4, No. 1, pp.1-23.

23. Kishida, Hideaki and Meyerhof, G. G.(1965). "Bearing capacity of pile groups eccentric loads in sand." Proc. 5^{th} Int. Conf. Soil Mech. Vol. 2, pp.270-274.

24. Kishida, Hideaki (1967), "Ultimate bearing capacity of piles driven into loose sand." Soil and Foundations, Vol. 7, No. 3, pp.20-29.

25. Lamb, T. William, and Whitman, Robert V. (1969). "Soil Mechanics." John Wiley & Sons.

26. Levacher, Daniel R., and Sieffert, Jean-Georges (1984). "Tests on model tension piles." J. of Geotech. Eng., Vol.110, No.12, pp.1735-1748.

27. Matlock, H. and Reese, L. C. (1962). "Generalized solutions for laterally loaded piles." ASCE, Transactions, Vol. 127, Part 1, pp.1220-1251.

28. Menzenbach, E. (1961). "The determination of the permissible point-load of piles by means of static penetration tests." Proc. 5th Int. Conf. on S. M. & F. E., Vol. 2, Paris, pp.99-104.

29. Meyerhof, G. G. (1951). "The ultimate bearing capacity of foundations." Geotechnique, Vol. 2, pp.301-332.

30. Meyerhof, G. G. (1953). "The bearing capacity of foundations under eccentric and inclined loads." Proc. 3rd Int. Conf. on S. M. & F. E., Vol. 1, session 4/24, Switzerland, pp.440-445.

31. Meyerhof, G. G. (1956). "Penetration tests and bearing capacity of cohesionless soils." ASCE, Vol. 82, No. SM1, pp.1-19.

32. Meyerhof, G. G. (1959). "Compaction of sands and bearing capacity of piles." ASCE, Vol. 85, No. SM6, pp.1-29.

33. Meyerhof, G. G. and Ranjan, Gopal (1972). "The bearing capacity of rigid piles under inclined loads in sand. 1: vertical piles." Can. Geotech. J. Vol.9, pp.430-446.

34. Meyerhof, G. G. (1973). "The uplift capacity of foundations under oblique loads." Can. Geotech. J., Vol. 10, pp.64-70.

35. Meyerhof, G. G. and Ranjan, Gopal (1973). "The bearing capacity of rigid piles under inclined loads in sand. 2: batter piles." Can. Geotech. J., Vol.10, pp.71-85.

36. Meyerhof, G. G. (1976). "Bearing capacity and settlement of pile foundations." ASCE, Vol. 102, No. GT3, pp.197-228.

37. Meyerhof, G. G. (1970). "Geotechnical properties of offshore soils." 1st Can. Conf. on Marine Geotech. Eng., Session 4, pp.1-8.

38. Meyerhof, G. G., Mathur, S. K. and Valsangkar, A. J. (1980). "Lateral

resistance and deflection of rigid walls and piles in layered soils." Can. Geotech. J., Vol.18, pp.159-170.

39. Meyerhof, G. G., Mathur, S. K. and Valsangkar, A. J. (1981). "The bearing capacity of rigid piles and pile groups under inclined loads in layered sand." Can. Geotech. J., Vol. 18, pp.514-519.

40. Meyerhof, G. G., Yalcin, A. Sahap and Mathur, Surendra K. (1983)." Ultimate pile capacity for eccentric inclined load." J. of Geotech. Eng., Vol. 109, No. 3, pp.408-423.

41. Mohan, Dinesh, Jain,G. S. and Kumar, V. (1963). "Load-bearing capacity of piles." Geotechnique, Vol. 13, pp.76-86.

42. Nordlund, R. L. (1963). "Bearing capacity of piles in cohesionless soils." ASCE, Vol. 89, No. SM3, pp.1-35.

43. Ohde, J. (1938). "The theory of earth pressure with special reference to earth pressure distribution." Bautechnik 16.

44. Petrasovits, G. and Awad, A. (1972). "Ultimate lateral resistance of a rigid pile in cohesionless soil." 5th European Conf. on S. M. & F. E., Vol. 1, pp.407-412.

45. Pontyondy, J. G. (1961). "Skin friction between various soils and construction materials." Geotechnique, Vol. 11, No. 4, pp.339-353.

46. Poulos, Harry G. (1971). "Behaviour of laterally loaded piles: 1 - single piles." ASCE, Vol. 97, No. SM5, pp.711-731.

47. Poulos, H. G. and Davis, E. H. (1980). "Pile foundation analysis and design." John Wiley & Sons.

48. Prandtle, L. (1920). "On the hardness of plastic bodies." Nachr. Kgl. Ges. Wiss Gottingen, Math-Phys. Kl.

49. Reissener, H. (1924). "The earth pressure problem." Proc. 1st Int. Conf. Appl. Mech.

50. Robinsky, E. I. and Morrison, C. F. (1964). "Sand displacement and compaction around model piles." Can. Geotech. J., Vol. 1, No. 2, pp.81-93.

51. Tavenas, Francois A. (1970). "Load tests results on friction piles in sand." Can. Geotech. J., Vol. 8, pp.7-22.

52. Terzaghi, Karl (1943). "Theoretical soil mechanics." John Wiley and sons, New York.

53. Terzaghi, Karl (1955). "Evaluation of coefficients of subgrade reaction." Geotechnique, Vol. 5, No. 4, pp.297-326.

54. Tomlinson, M. J. (1977). "Pile design and construction practice." A Viewpoint Publication.

55. Vesic, Aleksandar S. (1963), "Bearing capacity of deep foundations in sand."

Highway Res. Rec. No. 39, pp.112-153.

56. Vesic, Aleksandar S. (1964). "Investigations of bearing capacity of piles in sand." Proc. Conf. on Deep Foundations, Vol. 1, Mexico, pp.197-224.

57. Vesic, Aleksandar S. (1967). "Ultimate loads and settlements of deep foundations in sand." Proc. of a Symposium on Bearing Capacity and Settlement of Foundations, Duke University, pp.53-68.

58. Vesic, Aleksandar S. (1967). "A study of bearing capacity of deep foundations" George Institude of Technology, Georgia.

59. Vesic, Aleksandar S. (1977). "Design of pile foundations." Synthesis of Highway Pratice 42, Transportation Res. Rec.

60. Whitaker, Thomas (1957). "Experiments with model piles in groups." Geotechnique, Vol. 7, pp.147-167.

61. Whitaker, Thomas (1976). "The design of piled foundations." Pergamon Press.

62. Yoshimi, Yoshiaki (1964). "Piles in cohesionless soil subject to oblique pull." ASCE, Vol. 90, No. SM6, pp.11-24.

APPENDIX

COMPUTER PROGRAMS

```
5      REM *************** JMTEST ***********************
10     REM **** PROGRAM TO MEASURE PRESSURES ON *******
.      ******** PRESSURE TRANDUCERS & LOAD CELLS ******
20     DIM BDATA$[488],CDATA$[488],TL(11),BL(11),P1(11),
.      P2(11),P3(11),P4(11),P5(11),P6(11),P7(11),P8(11),
.      P9(11),P10(11),P11(11),P12(11),P13(11),P14(11),
.      MULTPLX(22)!
30     DIM TLAVG(25),BLAVG(25),P1AVG(25),P2AVG(25),P3AVG
.      (25),P4AVG(25),P5AVG(25),P6AVG(25),P7AVG(25),P8AVG
.      (25),P9AVG(25),P10AVG(25),P11AVG(25),P12AVG(25),
.      P13AVG(25),P14AVG(25),D(25)!
40     DISP "INPUT NUMBER OF LOAD READINGS TO BE TAKEN
.      (=NLR)"
50     INPUT NLR
60     REM *** NUMBER OF DATA PER CHANNEL (NDP=10) ****
70     NDP=10
80     DISP "INPUT THE NUMBER OF CHANNELS (NC=PT'S+LC'S
.      LVDT'S)"
90     INPUT NC
100    CREATE "PILE",20,256
110    ASSIGN# 1 TO "PILE"
120    REM **** START LOOP TO MEASURE PRESSURES *****
130    FOR J=1 TO NLR
140    DISP "INPUT DEPTH (cm or turns)"
150    INPUT D(J)
160    REM ************** READ DATA *******************
170    IOBUFFER BDATA$
180    DISP "Reading data from 3497A for BDATA$"
190    CLEAR 509
200    OUTPUT 509 ;"VF2VA0VR2VT2SD0"
210    OUTPUT 509 ;"S01VN1AF2AL11AE1AC2T02"
220    REM ***** TRANSFER DATA TO FILE USING FHS *****
230    TRANSFER 509 TO BDATA$ FHS
240    LOCAL 509 @CLEAR 509 @BEEF 10,100
250    DISP "Data transfer complete"
260    IF NC<=10 THEN GOTO 370
270    DISP "NC>10"
280    IOBUFFER CDATA$
290    DISP "Reading data from 3497A for CDATA$"
300    CLEAR 509
310    OUTPUT 509 ;"VF2VA0VR2VT2SD0"
320    OUTPUT 509 ;"S01VN1AF12AL17AE1AC12T02"
330    TRANSFER 509 TO CDATA$ FHS
340    LOCAL 509 @CLEAR 509 @BEEP 10,100
350    REM ************* UNPACKING DATA ***************
360    DISP "Unpacking data. Please wait"
370    FOR I=3 TO 3*NDP*NC STEP 3
380    IF I>3*NDP*10 THEN GOTO 570
390    A$=DTB$(NUM(BDATA$[I-2,I-2]))
400    D$=A$
410    A2=BINAND(BDT(A$[9,10],3)
420    M=10**(-6+A2) ! Range multipler
430    IF BINAND (BTD(A$[11,11],1)=1 THEN SIGN=-1 ELSE
.      SIGN=1
```

```
440      ORNG=BINAND (BTD(A$[12,12]),1) ! Overange bit
450      MSD=BINAND (BTD(A$[13,16]),15)
460      A$=DTB$(NUM(BDATA$[I-1,I-1]))
470      B$=A$
480      SSD=BINAND(BTD(A$[9,12]),15)
490      TSD=BINAND(BTD(A$[13,16]),15)
500      A$=DTB(NUM(BDATA$[I,I]))
510      C$=DTB(NUM(BDATA$[I,I]))
520      FSD=BINAND(BTD(A$[9,12]),15)
530      LSD=BINAND(BTD(A$[13,16]),15)
540      MULTPLX(I/3)=(ORNG*10**5+MSD*10**4+SSD*10**3+TSD
.        *10**2+FSD*10+LSD)*M*SIGN
550      NEXT I
560      GOTO 750
570      FOR I=3*NDP*10+3 TO 3*NDP*NC+6 STEP 3
580      A$=DTB$(NUM(CDATA$[I-2,I-2]))
590      D$=A$
600      A2=BINAND(BTD(A$[9,10]),3)
610      M=10**(-6+A2)
620      IF BINAND(BTD(A$[11,11]),1)=1 THEN SIGN=-1 ELSE
.        SIGN=1
630      ORNG=BINAND(BTD(A$[12,12]),1)
640      MSD=BINAND(BTD(A$[13,16]),15)
650      A$=DTB$(NUM(CDATA$[I-1,I-1]))
660      B$=A$
670      SSD=BINAND(BTD(A$[9,12]),15)
680      TSD=BINAND(BTD(A$[13,16]),15)
690      A$=DTB$(NUM(CDATA$[I,I]))
700      C$=DTB$(NUM(CDATA$[I,I]))
710      FSD=BINAND(BTD(A$[9,12]),15)
720      LSD=BINAND(BTD(A$[13,16]),15)
730      MULTPLX(I/3)=(ORNG*10**5+MSD*10**4+SSD*10**3+TSD
.        *10**2+FSD*10+LSD)*M*SIGN
740      NEXT I
750      CALO=1
760      REM ************ DEMULTPLEX ********************
770      C1=1
780      FOR I=1 TO NDP
790      TL(I)=MULTPLX(C1)*CALO @C1=C1+1
800      BL(I)=MULTPLX(C1)*CALO @C1=C1+1
810      P1(I)=MULTPLX(C1)*CALO @C1=C1+1
820      P2(I)=MULTPLX(C1)*CALO @C1=C1+1
830      P3(I)=MULTPLX(C1)*CALO @C1=C1+1
840      P4(I)=MULTPLX(C1)*CALO @C1=C1+1
850      P5(I)=MULTPLX(C1)*CALO @C1=C1+1
860      P6(I)=MULTPLX(C1)*CALO @C1=C1+1
870      P7(I)=MULTPLX(C1)*CALO @C1=C1+1
880      P8(I)=MULTPLX(C1)*CALO @C1=C1+1
890      NEXT I
900      C1=NDP*10+3
910      FOR I=1 TO NDP
920      P9(I)=MULTPLX(C1)*CALO @C1=C1+1
930      P10(I)=MULTPLX(C1)*CALO @C1=C1+1
940      P11(I)=MULTPLX(C1)*CALO @C1=C1+1
```

```
950      P12(I)=MULTPLX(C1)*CALO @C1=C1+1
960      P13(I)=MULTPLX(C1)*CALO @C1=C1+1
970      P14(I)=MULTPLX(C1)*CALO @C1=C1+1
980      NEXT I
990      N$="NO" @TL$="TOP L" @BL$="BOTTOM L" @P1$=
.        "PT1" @P2$="PT2" @P3$="PT3" @P4$="PT4" @P5$=
.        "PT5" @P6$="PT6"
1000     PRINT USING 1010; N$,TL$,BL$,P1$,P2$,P3$,P4$,
.        P5$,P6$
1010     IMAGE 4A,10A,10A,10A,10A,10A,9A,9A,9A
1020     FOR I=1 TO NDP
1030     PRINT USING 1040;I,TL(I),BL(I),P1(I),P2(I),P3
.        (I),P4(I),P5(I),P6(I)
1040     IMAGE 2D,2X,SD.5D,2X,SD.5D,2X,SD.5D,2X,SD.5D,2X,
.        SD.5D,1X,SD.5D,1X,SD.5D,1X,SD.5D
1050     NEXT I
1060     N$="NO" @P7$="PT7" @P8$="PT8" @P9$="PT9" @P
.        10$="PT10" @P11$="PT11" @P12$="PT12" @LV1$="R.
.        DEF" @LV2$="H.DEF"
1070     PRINT USING 1080 ;N$,P7$,P8$,P9$,P10$,P11$,P12$,
.        LV1$,LV2$
1080     IMAGE 4A,10A,10A,9A,9A,9A,9A,10A,10A
1090     FOR I=1 TO NDP
1000     PRINT USING 1110;I,P7(I),P8(I),P9(I),P10(I),
.        P11(I),P12(I),P13(I),P14(I)
1110     IMAGE 2D,2X,SD.5D,2X,SD.5D,1X,SD.5D,1X,SD.5D,1X,
.        SD.5D,1X,SD.5D,1X,SDD.5D,1X,SDD.5D
1120     NEXT I
1130     REM ************* AVERAGE READING**************
1140     TL(0)=0 @BL(0)=0 @P1(0)=0 @P2(0)=0 @P3(0)=0,
.        P4(0)=0 @P5(0)=0 @P6(0)=0 @P7(0)=0 @P8(0)=0 @P9
.        (0)=0 @P10(0)=0 @P11(0)=0 @P12(0)=0 @P13(0)=0
.        @P14(0)=0
1150     FOR I=1 TO NDP
1160     TL(I)=TL(I-1)+TL(I)
1170     BL(I)=BL(I-1)+BL(I)
1180     P1(I)=P1(I-1)+P1(I)
1190     P2(I)=P2(I-1)+P2(I)
1200     P3(I)=P3(I-1)+P3(I)
1210     P4(I)=P4(I-1)+P4(I)
1220     P4(I)=P4(I-1)+P4(I)
1230     P5(I)=P5(I-1)+P5(I)
1240     P6(I)=P6(I-1)+P6(I)
1250     P7(I)=P7(I-1)+P7(I)
1260     P8(I)=P8(I-1)+P8(I)
1270     P9(I)=P9(I-1)+P9(I)
1280     P10(I)=P10(I-1)+P10(I)
1290     P11(I)=P11(I-1)+P11(I)
1300     P12(I)=P12(I-1)+P12(I)
1310     P13(I)=P13(I-1)+P13(I)
1320     P14(I)=P14(I-1)+P14(I)
1330     NEXT I
1340     TLAVG(J)=TL(NDP)/NDP
1350     BLAVG(J)=BL(NDP)/NDP
```

```
1360    P1AVG(J)=P1(NDP)/NDP
1370    P2AVG(J)=P2(NDP)/NDP
1380    P3AVG(J)=P3(NDP)/NDP
1390    P4AVG(J)=P4(NDP)/NDP
1400    P5AVG(J)=P5(NDP)/NDP
1410    P6AVG(J)=P6(NDP)/NDP
1420    P7AVG(J)=P7(NDP)/NDP
1430    P8AVG(J)=P8(NDP)/NDP
1440    P9AVG(J)=P9(NDP)/NDP
1450    P10AVG(J)=P10(NDP)/NDP
1460    P11AVG(J)=P11(NDP)/NDP
1470    P12AVG(J)=P12(NDP)/NDP
1480    P13AVG(J)=P13(NDP)/NDP
1490    P14AVG(J)=P14(NDP)/NDP
1500    REM *********** STORE DATA ********************
1510    PRINT# 1;J,D(J),TLAVG(J),BLAVG(J),P1AVG(J),P2AVG
.       (J),P3AVG(J),P4AVG(J),P5AVG(J),P6AVG(J),P7AVG(J),
.       P8AVG(J),P9AVG(J),P10AVG(J),P11AVG(J),P12AVG(J),
.       P13AVG(J),P14AVG(J)
1520    NEXT J
1530    ASSIGN# 1 TO *
1540    PRINT; " "
1550    N$="NO" @D$="DEPTH" @TL$="TOP L" @BL$="BOTTOM"
.       @P1$="PT1" @P2$="PT2" @P3$="PT3" @P4$="PT4" @P5
.       $="PT5" @P6$="PT6"
1560    PRINT USING 1570; N$,D$,TL$,BL$,P1$,P2$,P3$,P4$,
.       P5$,P6$
1570    IMAGE 4A,8A,8A,8A,8A,8A,8A,8A,8A,8A
1580    FOR J=1 TO NLR
1590    PRINT USING 1600; J,D(J),TLAVG(J),BLAVG(J),P1AVG
.       (J),P2AVG(J),P3AVG(J),P4AVG(J),P5AVG(J),P6AVG(J)
1600    IMAGE 2D,2X,6D,1X,S.5D,1X,S.5D,1X,S.5D,1X,S.5D,1X,
.       S.5D,1X,S.5D,1X,S.5D,1X,S.5D
1610    NEXT J
1620    N$="DEPTH"@P7$="PT7"@P8$="PT8"@P9$="PT9"@P10
.       ="PT10" @P11$="PT11" @P12$="PT12" @LV1$="R.DEF"
.       @LV2$="H.DEF"
1630    PRINT USING 1640; N$,P7$,P8$,P9$,P10$,P11$,P12$,
.       LV1$,LV2$
1640    IMAGE 4A,10A,10A,9A,9A,9A,9A,10A,10A
1650    FOR I=1 TO NLR
1660    PRINT USING 1670;D(I),P7AVG(I),P8AVG(I),P9AVG(I),
.       P10AVG(I),P11AVG(I),P12AVG(I),P13AVG(I),P14AVG(I)
1670    IMAGE 2D,2X,SD.5D,2X,SD.5D,1X,SD.5D,1X,SD.5D,1X,
.       SD.5D,1X,SD.5D,1X,SDD.5D,1X,SDD.5D
1680    NEXT I
1690    END
```

```
10      REM ****** PROGRAM TO DRAW LATERAL PRESSURE ******
.       ********** DISTRIBUTION CURVE ********************
20      DIM BY(9,100),BZ(9,100),E(9),CZ(600),CY(600),
.       FX(600),FY(600),YY(12),H(9),F(9),X(12),Y(12),
.       P(9),G(9,9),A(9),B(9),C(9),D(9)
30      PLOTTER IS 505
40      DISP "IF YOU DON'T WANT TO DRAW FRAME,LIFT PEN UP"
50      PAUSE
60      DISP "PRESS (CONTINUE) TO CONTINUE"
70      LOCATE 20,120,20,90
80      SCALE -200,200,900,0
90      DEG
100     FXD 0,0
110     LGRID -10,50,0,900,10,4
120     MOVE -50,990
130     LDIR 0
140     CSIZE 3
150     LABEL "SOIL PRESSURE (kPa)"
160     MOVE -260,450
170     LDIR 90
180     LABEL "DEPTH (mm)"
190     MOVE 60,-30
200     LDIR 0
210     LABEL "B=102 mm"
220     MOVE 150,-30
230     LDIR 0
240     LABEL "0=30"
250     MOVE 150,-30
260     LDIR 0
270     LABEL "-=30"
280     MOVE -40,-30
290     LDIR 0
300     LABEL "D=900 mm"
310     FRAME
320     DISP "IF YOU WANT TO PLOT DATA,TAKE PEN DOWN"
330     PAUSE
340     DISP "PRESS (CONTINUE) TO CONTINUE"
350     DISP "ENTER NUMBER OF DATA (N)"
360     INPUT N
370     FOR J=1 TO N
380     DISP "ENTER DATA POINTS (X(J) in kPa, Y(J) in mm)"
390     INPUT X(J),Y(J)
400     NEXT J
410     FOR I=1 TO N-1
420     H(I)=X(I+1)-X(I)
430     F(I)=Y(I+1)-Y(I)
440     NEXT I
450     FOR I=2 TO N-1
460     P(I)=(F(I)/H(I)-F(I-1)/H(I-1))*6
470     NEXT I
480     P(1)=0 @P(N)=0
490     FOR I=1 TO N
500     FOR J=1 TO N
510     G(I,J)=0
```

```
520     NEXT J
530     NEXT I
540     FOR I=2 TO N-1
550     G(I,I)=2*(H(I-1)+H(I))
560     G(I,I-1)=H(I-1)
570     G(I,I+1)=H(I)
580     NEXT I
590     G(1,1)=H(2)
600     G(1,2)=-(H(1)+H(2))
610     G(1,3)=H(1)
620     G(N,N-2)=H(N-1)
630     G(N,N-1)=-(H(N-2)+H(N-1))
640     G(N,N)=H(N-2)
650     REM ****** OBTAIN THE INVERSION MATRIX AND ******
.       ********** THE VALUE OF Y ***********************
660     FOR K=1 TO N
670     FOR J=1 TO N
680     IF J=K THEN GOTO 700
690     G(K,J)=G(K,J)/G(K,K)
700     NEXT J
710     G(K,K)=1/G(K,K)
720     FOR I=1 TO N
730     IF I=K THEN GOTO 780
740     FOR J=1 TO N
750     IF J=K THEN GOTO 770
760     G(I,J)=G(I,J)-G(K,J)*G(I,K)
770     NEXT J
780     NEXT I
790     FOR I=1 TO N
800     IF I=K THEN GOTO 820
810     G(I,K)=-(G(I,K)*G(K,K))
820     NEXT I
830     NEXT K
840     FOR I=1 TO N
850     E(I)=0
860     FOR J=1 TO N
870     E(I)=E(I)+G(I,J)*(P(J)
880     NEXT J
890     NEXT I
900     FOR I=1 TO N
910     PRINT;E(I)
920     NEXT I
930     REM ******** FIND THE COEFFICIENTS A,B,C,AND D ***
.       ************ FOR EACH INTERVALS ******************
940     FOR I=1 TO N-1
950     B(I)=E(I)/2
960     A(I)=(E(I+1)-E(I))/(6*H(I))
970     C(I)=F(I)/H(I)-(2*H(I)*E(I)+H(I)*E(I+1))/6
980     D(I)=Y(I)
990     NEXT I
1000    PRINT ;"       GIVEN DATA"
1010    PRINT ;"DEPTH (mm)","SOIL PRESSURE (kPa)"
1020    FOR I=1 TO N
1030    PRINT X(I),Y(I)
```

```
1040    NEXT I
1050    PRINT; " "
1060    FOR I=1 TO N-1
1070    SUMA=0
1080    Z=X(I)
1090    M=20
1100    DZ=H(I)/M
1110    FOR J=1 TO M
1120    AY=A(I)*(Z-X(I))**3+B(I)*(Z-X(I))**2+C(I)*(Z-
.       X(I))+D(I)
1130    BY(I,J)=AY
1140    BZ(I,J)=Z
1150    Z=Z+DZ
1160    NEXT J
1170    NEXT I
1180    PRINT ;" "
1190    PRINT ;"       THE CALCULATED DATA"
1200    PRINT ;"DEPTH (mm)","SOIL PRESSURE (kPa)"
1210    k=1
1220    FOR I=1 TO N-1
1230    FOR J=1 TO M
1240    CZ(I)=BZ(I,J)
1250    CY(I)=BY(I,J)
1260    FX(K)=CZ(I)
1270    FY(K)=CY(I)
1280    PRINT ;FX(K),FY(K)
1290    K=K+1
1300    NEXT J
1310    NEXT I
1320    REM ****** PLOT DATA ON THE PLOTTER *********
1330    DISP "ENTER CHARACTER STRING"
1340    INPUT C$
1350    LORG 5
1360    FOR I=1 TO M*(N-1)
1370    PLOT FY(I),FX(I)
1380    NEXT I
1390    DISP "DO YOU WANT TO PUT DATA POINTS ON ?
.       (YES/NO)"
1400    INPUT PL$
1410    IF PL$="YES" THEN GOTO 1420 ELSE GOTO 1460
1420    DISP "ENTER DATA POINTS (DEPTH, PRESSURE)"
1430    INPUT X,Y
1440    MOVE Y,X @LABEL C$
1450    GOTO 1390
1460    DISP "DO YOU WANT TO LABEL ? (YES/NO)"
1470    INPUT YN$
1480    IF YN$="YES" THEN GOTO 1490 ELSE GOTO 1610
1490    DISP "INPUT COORDINATES AT CENTER OF LABEL; X,Y"
1500    INPUT X,Y
1510    MOVE X,Y
1520    DISP "INPUT LABEL DIRECTION IN DEGREE"
1530    INPUT D
1540    DEG @LDIR D
1550    DISP "INPUT LABEL"
```

```
1560     INPUT L$
1570     DISP "INPUT CHARACTER SIZE"
1580     INPUT S
1590     CSIZE S
1600     LABEL L$
1610     DISP "DO YOU WANT TO LABEL MORE ? (YES/NO)"
1620     INPUT YO$
1630     IF YO$="YES" THEN GOTO 1490 ELSE GOTO 1640
1640     DISP "DO YOU WANT TO GET ANOTHER DATA FILE ?
.        (YES/NO)"
1650     INPUT YE$
1660     IF YE$="YES" THEN GOTO 350 ELSE GOTO 1670
1670     DUMP GRAPHICS
1680     END
```